SANDIA REPORT

SAND2014-0186
Unlimited Release
Printed January 2014

Understanding the Function and Performance of Carbon-enhanced Lead-acid Batteries

Final Report

D.G. Enos, S.R. Ferreira, R. Shane

Prepared by
Sandia National Laboratories
Albuquerque, New Mexico 87185 and Livermore, California 94550

Sandia National Laboratories is a multi-program laboratory managed and operated by Sandia Corporation, a wholly owned subsidiary of Lockheed Martin Corporation, for the U.S. Department of Energy's National Nuclear Security Administration under contract DE-AC04-94AL85000.

Issued by Sandia National Laboratories, operated for the United States Department of Energy by Sandia Corporation.

Available to DOE and DOE contractors from
U.S. Department of Energy
Office of Scientific and Technical Information
P.O. Box 62
Oak Ridge, TN 37831

Telephone: (865) 576-8401
Facsimile: (865) 576-5728
E-Mail: reports@adonis.osti.gov
Online ordering: http://www.osti.gov/bridge

Available to the public from
U.S. Department of Commerce
National Technical Information Service
5285 Port Royal Rd.
Springfield, VA 22161

Telephone: (800) 553-6847
Facsimile: (703) 605-6900
E-Mail: orders@ntis.fedworld.gov
Online order: http://www.ntis.gov/help/ordermethods.asp?loc=7-4-0#online

SAND2014-0186
Unlimited Release
Printed January 2014

Understanding the Function and Performance of Carbon-enhanced Lead-acid Batteries

D. G. Enos
Materials Reliability Department
Sandia National Laboratories
Albuquerque, NM 87185

Summer R. Ferreira
Advanced Power Sources R&D Department
Sandia National Laboratories
Albuquerque, NM 87185

R. Shane
East Penn Manufacturing
Lyon Station, PA 19536

Abstract

This report describes the status of research being performed under CRADA No. SC10/01771.00 (Lead/Carbon Functionality in VRLA Batteries) between Sandia National Laboratories and East Penn Manufacturing, conducted for the U.S. Department of Energy's Energy Storage Systems Program. Past studies have entailed phenomenological research observing that carbon additions prevent/reduce sulfation of the negative electrode; however, no understanding is available to provide insight into why certain carbons are successful while others are not. Impurities were implicated in one recent review of the electrochemical behavior of carbon additions. In this work, control cells along with three different carbon modified cells were evaluated under a range of conditions, from basic electrochemical performance through high rate, partial state of charge cycling. The physical and chemical changes taking place within the plates were monitored and an effort to correlate performance to those changes was made.

ACKNOWLEDGMENTS

The authors would like to acknowledge the significant technical support provided by Wes Baca for testing and cell disassembly, Bonnie McKenzie for assistance with SEM and cathodoluminescence imaging, Denise Bencoe for BET and Hg Porosimetry measurements, Alice Kilgo for metallographic analyses, Mark Rodriguez for x-ray diffraction, and Ted Borek for soluble contaminant analysis, along with helpful technical discussions with Tom Hund and Kyle Fenton.

CONTENTS

FIGURES

TABLES

NOMENCLATURE

1C	Capacity at the 1 hour rate
Ah	Amp-hours
ALABC	Advanced Lead Acid Battery Consortia
BET	Brunauer, Emmet, and Teller surface area
CSIRO	Commonwealth Scientific and Industrial Research Organisation
DOE	Department of Energy
HPPC	Hybrid Pule Power Characterization
HRPSoC	High Rate, Partial State of Charge
ICP-MS	Inductively Coupled Plasma – Mass Spectroscopy
N	Normality (moles solute per kg solvent)
NAM	Negative Active Material
Pb-C	Lead-carbon battery
ppm	parts per million
SEM	Scanning electron microscopy
SOC	State of Charge
SNL	Sandia National Laboratories
V	Voltage
VRLA	Valve Regulated Lead Acid
VPSE	Variable pressure secondary electron

PROJECT DESCRIPTION

Carbon has been explored as an addition to lead-acid battery electrodes in a number of ways. Perhaps the most notable to date has been the hybrid "Ultrabattery" developed by CSIRO where an asymmetric carbon-based electrochemical capacitor is combined with a lead-acid battery into a single cell, dramatically improving high-rate partial-state-of-charge (HRPSoC) operation. (Lam, et al., 2007). As illustrated below (Figure 1), the "Ultrabattery" is a hybrid device constructed using a traditional lead-acid battery positive plate (*i.e.*, PbO_2) and a negative electrode consisting of a carbon electrode in parallel with a lead-acid negative plate:

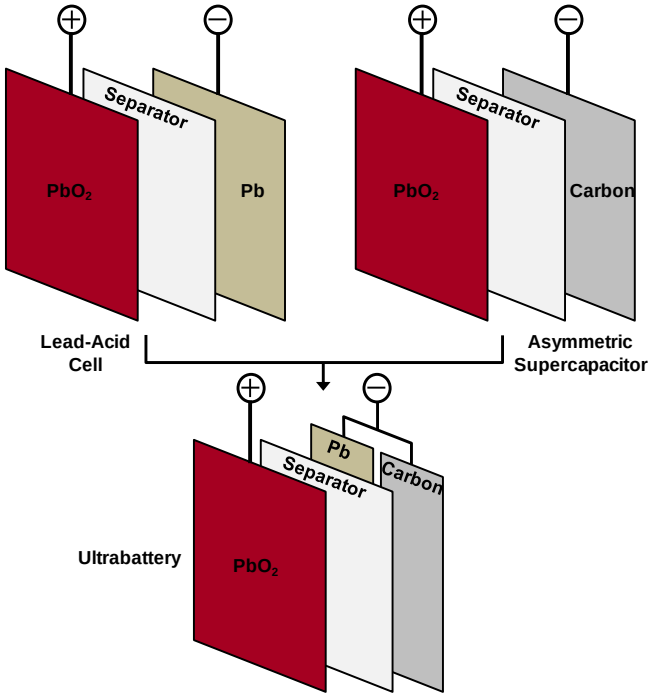

Figure 1: Schematic representation of a single cell from the Ultrabattery (after Lam et al. 2007)

This device exhibits a dramatically improved cycle life over traditional VRLA batteries, as well as increased charge power and charge acceptance. The "Ultrabattery" has been produced successfully by both The Furukawa Battery Co. and East Penn Manufacturing. An example illustrating the dramatic improvement in cycle life of the Ultrabattery over a conventional VRLA battery is shown in the graph below:

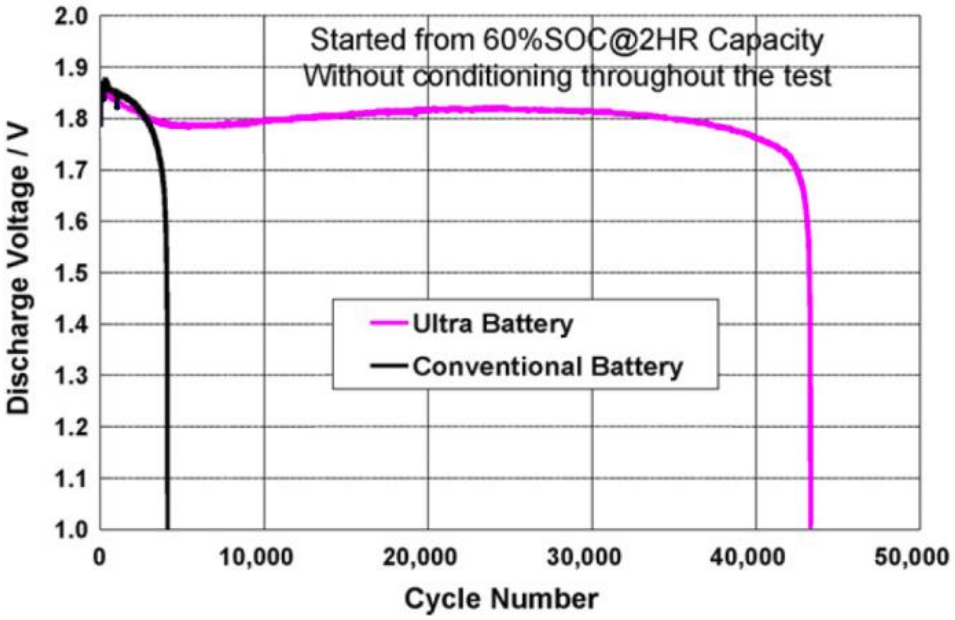

Figure 2: Discharge voltage as a function of number of cycles under the EUCAR cycle life test. (Lam, et al., 2007.)

In addition to the aforementioned hybrid device, carbon has also been added directly to traditional VRLA batteries as an admixture in both the positive and negative plates, the latter of which has been found to result in similar improvements to battery performance under high-rate partial-state-of-charge (HRPSoC) operation (Figure 2). It is this latter construction, where carbon is added directly to the negative active material (NAM) that is the specific design being evaluated through this program. Thus, the carbon-modified (or Pb-C) battery (termed the "Advanced" VRLA battery by East Penn Manufacturing) is a traditional VRLA battery where an additional component has been added to the negative electrode during production of the negative plate (Figure 3).

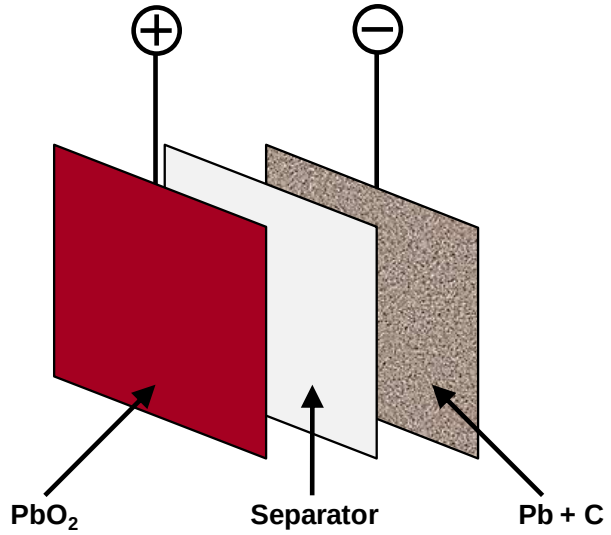

Figure 3: Schematic representation of a single cell from a carbon-modified or "Advanced" VRLA battery.

The addition of select carbon materials to the NAM of VRLA batteries has been demonstrated to increase cycle life by an order of magnitude or more under (HRPSoC) operation. Additionally, battery capacity increases on cycling and, in fact, exceeds the performance of the batteries when new (Figure 4).

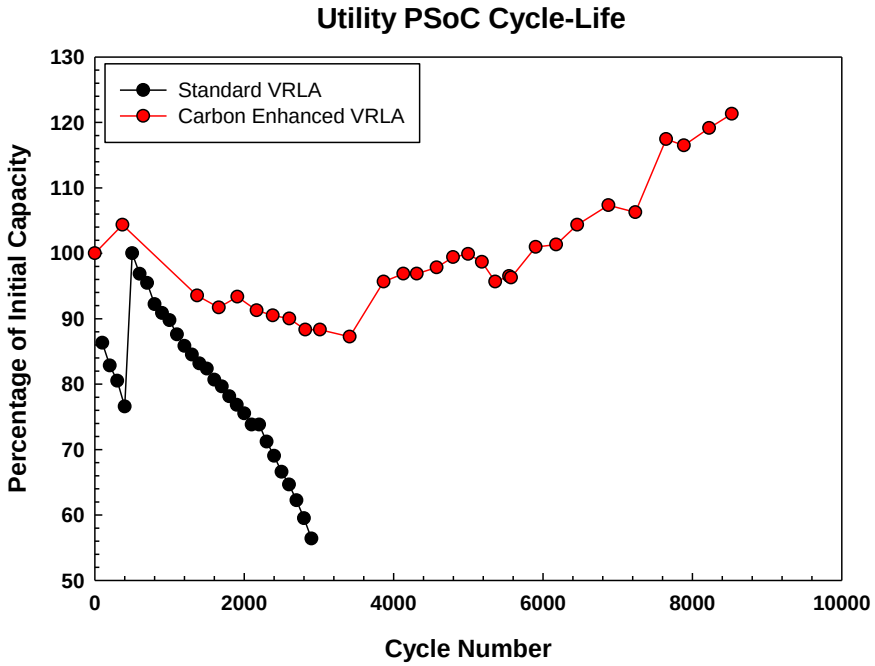

Figure 4: Capacity as a function of cycle life for a commercially available, conventional VRLA, and a carbon-modified VRLA battery where carbon has been added to the NAM. (the increase in capacity observed at 400 cycles for the standard battery was the result of a recovery charging procedure)

Physically, the mechanism by which carbon extends battery life is generally accepted to be through reduction/elimination of sulfation of the negative electrode (Figure 5). Sulfation is a process that results in the formation of lead sulfate ($PbSO_4$) crystals that are electrically isolated from the lead in the electrode, and thus are unable to be electrochemically reduced through the recharging process. These $PbSO_4$ crystals eventually block the surface, dramatically reducing the capacity of the negative plate (Figure 5, left). The carbon additives lead to reduced sulfation at the plate surface, extending the life to when failure occurs uniformly throughout the plate cross-section (Figure 5, right). It is not clear why some carbons produce this effect and others do not.

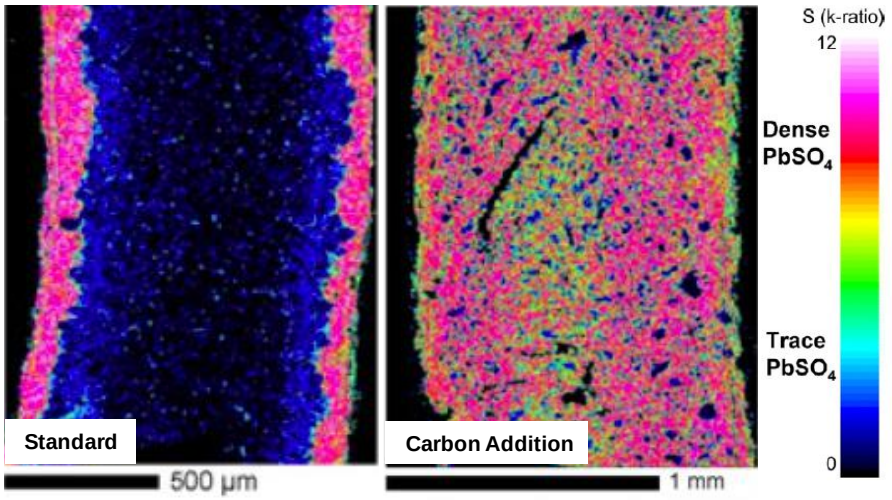

Figure 5: Elimination of hard sulfation by carbon additions, allowing more complete usage of the battery (both images are from cells at end of life). Fernandez et al., 2010.

The underlying mechanism responsible for improving capacity on cycling is not known. Developing an understanding of the fundamental physical, chemical, and electrochemical mechanisms underlying both aspects of enhanced performance offers the possibility of significantly improving VRLA batteries by intentionally designing and fabricating electrode structures with superior performance. Furthermore, once understood at a fundamental level, it may be possible to extend this approach to other battery chemistries. In this collaborative effort with East Penn Manufacturing, we will investigate the fundamental physicochemical basis and structure-activity relationships underlying carbon-enhanced VRLA batteries.

This program focuses on 1) developing a fundamental physical, chemical, and electrochemical understanding of the mechanism of enhanced performance of carbon-enhanced VRLA batteries; 2) demonstrating this understanding by fabricating batteries exhibiting optimum performance; and 3) determining to what extent this approach can be applied to other battery chemistries.

Engineering the enhanced performance of PbC batteries will ultimately lead to reduced life-cycle cost, which is an enabling factor for many stationary applications including utility ancillary regulation services, wind farm energy smoothing, and solar photovoltaic energy smoothing.

BACKGROUND

Much of the research presented in the literature that discusses the effect of carbon additions to the NAM focuses primarily on the phenomenological observations (*i.e.*, cycle life increases, resistance to hard sulfation increases) rather than postulating/exploring potential mechanisms through which the effect is achieved. A summary of recent work from groups attempting to establish the mechanisms through which carbon enhances the performance of VRLA batteries is presented below.

Looking first to the work of Shiomi, *et al* (Shiomi, Funato, Nakamura, Takahash, & Tsubota, 1997) where the beneficial effect of carbon added to the NAM was first reported, it was proposed that carbon forms a conductive network between $PbSO_4$ crystals, leading to an enhancement in the rechargability of the negative plate. Ohmae, *et al.* expressed a similar view, in that a highly conductive carbon was a necessary addition to the NAM in order to retard the sulfation process. (Ohmae, Hayashi, & Inoue, 2003) In other words, the carbon served as a conductor, hindering the formation of $PbSO_4$ crystals that were electrically isolated from the metallic lead within the plate, and thus not able to be reduced during the recharging process. While Shiomi and Ohmae believe that the electrical conductivity of the carbon addition is the critical aspect, other researchers, such as Spence, *et al.*, have found that neither electrical conductivity nor surface reactivity were important in determining the effect of a carbon addition to the NAM (Spence, Boden, & Wojcinski, 2008).

Spence, *et* al., argued instead that the beneficial impact of the carbon was due to the alteration of the pore structure of the NAM, enabling electrolyte to be banked within the pore structure, and thus available within the NAM, rather than having to diffuse from the surface (Spence, Boden, & Wojcinski, 2009). They concluded that any addition, not just carbon, which modified the pore structure in such a manner would result in an improvement in performance. This theory is supported by Calebeck and Micka, *et al.* (Calábek, et al., 2008) (Micka, et al., 2009) (Calebek, Micka, Krivak, & Baca, 2006) where both titania (TiO_2) and alumina (Al_2O_3) were found to provide improvements similar to those obtained by carbon, though their argument was that, in addition to obstructing large pores in the NAM, the additions hindered growth of $PbSO_4$ crystals, preventing the formation of the large crystallites associated with sulfation. Valenciano, *et al*. also observed a beneficial effect of an inert addition, in their case glass fibers, though the resulting improvement appeared to depend on the manner in which the battery itself was assembled (Valenciano, Sanchez, Trinidad, & Hollenkamp, 2006).

As with Shiomi, Boden, *et al*. (Boden, Loosemore, Spence, & Wojcinski, 2010) observed that the cycle life was increased by eliminating surface buildup of $PbSO_4$ on the negative electrode (*i.e.*, hard sulfation), and also hypothesized that the increased capacity of the carbon-modified battery was due to the increased electrochemical efficiency of the NAM brought about by the more thorough use of the electrode. Boden also reported that metallic lead clusters were observed on the surface of carbon particles, indicating that the soluble lead ions were electrochemically reduced on the carbon surface in the same way as they are on lead surfaces. A number of other researchers have presented results that support the theory that carbon acts as a nucleation site for the recharging process, improving utilization of the NAM. Kozawa, *et al*. explored the addition of colloidal carbon to the electrolyte of a sulfated battery, where they observed that the battery could be electrochemically recovered, with the carbon adsorbing (i.e., depositing) onto the NAM and acting as a nucleation site for Pb deposition during charge (Kozawa, Oho, Sano, Brodd, & Brodd, 1999). Pavlov, *et al*. also expressed that carbon was electrochemically active in the NAM, providing additional surface area upon which charge/discharge reactions could take place (Pavlov, Nikolov, & Rogachev, Influence of Expander Components on the Processes at the Negative Plates of Lead-acid Cells on High-rate Partial-state-of-charge Cycling. Part II. Effect of Carbon Additives on the Processes of Charge and Discharge of Negative Plates, 2010). Finally, Boden reported that Brunauer-Emmett-Teller (BET) surface area measurements indicated that the surface area decreased with cycle life, suggesting that the carbon is becoming progressively buried under lead and $PbSO_4$ reaction products and,

consequently, losing its beneficial effects. The theory that the carbon serves as an additional electroactive material in the NAM is in contrast to the results reported above by Spence *et al*., where surface reactivity did not appear to be important.

In a recent review of the effects of carbon on the electrochemical behavior of the negative active mass in a lead-acid battery, Moseley offered a number of potential mechanisms through which the performance could be increased. (Moseley, Nelson, & Hollenkamp, The Role of Carbon in Valve-regulated Lead-acid Battery Technology, 2006) (Moseley, Consequences of Including Carbon in the Negative Plates of Valve-regulated Lead-acid Batteries Exposed to High-rate Partial-state-of-charge Operation, 2009) First, he suggested that the carbon may increase the electrical conductivity of the NAM, facilitating the recharging process (*i.e.*, easing reduction of $PbSO_4$ in the NAM). Another potential mechanism would be the restriction of $PbSO_4$ crystal growth, which constrains the size of $PbSO_4$ crystals and enhances their dissolution rate during recharge, again facilitating the reduction of $PbSO_4$ during recharge. The latter effect has been demonstrated for a series of inert materials, such as titanium oxide (TiO_2) as discussed above. A potential mechanism for the increase in capacity that Moseley put forward was that the carbon could be acting as a capacitive component, much like in electrochemical capacitors, adding a capacitive energy storage component to the battery. The addition of a capacitive component was also presented by Fernandez, *et al*. (Fernandez, Valenciano, Trinidad, & Munoz, 2010) who attributed the dramatic improvement they observed in charge acceptance to the capacitive effect. Moseley also indicated a potential detrimental effect of carbon additions—if their impurity level is high, the impurities may facilitate detrimental side reactions (*e.g.*, such as water reduction) resulting in a loss of capacity.

Pavlov's group has also conducted significant research in this area. (Pavlov, Rogachev, Nikolov, & Petkova, 2009) Their overall theory is similar to that put forth by Boden, where during recharge two parallel processes take place with lead being reduced both on lead surfaces within the NAM as well as on carbon surfaces within the NAM. Thus, the effect of the carbon is to increase the overall electrochemically active surface area within the negative plate, thereby increasing its capacity and facilitating more complete recharge. Pavlov also found that carbon acted to reduce the pore size within the NAM, and that once the pores were reduced to below approximately 1.5 µm the diffusion of sulfuric acid (H_2SO_4) into the pores was impeded, and lead oxide (PbO), not $PbSO_4$, formed during operation.

In addition to the number of theories concerning how carbon affects the electrochemical behavior of a VRLA battery, there are a similar number of views as to what the appropriate form of the carbon is. Researchers have found that various forms of graphitic carbon, carbon black, and activated carbon have worked, although the results between researchers appear to vary. For example, Spence, *et al*. found that the best performance was observed for flake graphite, while Valenciano, *et al.* determined that flake graphite was detrimental to performance. Seemingly in support of the results of Spence, Sawai, *et al*. (Sawa, et al., 2006) explored the use of carbon particulate and fiber, finding that the larger fibrous material was not able to provide an increase in performance. Further, there have been comprehensive studies where numerous forms of carbon were evaluated, such as that reported by Walmet, where none of the materials (a series of flake graphites, expanded graphites, carbon blacks, or activated carbons) was able to provide an appreciable increase in performance, and in many cases, reduced performance relative to an unmodified control (Walmet, 2009).

Clearly, there is considerable variation from researcher to researcher in terms of both which carbons appear to work and the mechanism by which any beneficial effect that is observed has been achieved. This variability suggests that there may be other factors, such as how the battery was produced (*e.g.*, negative electrode paste formulation, plate production, battery activation, *etc.*), that play a major role in determining not only which carbons are beneficial, but also the role that they play in the battery's electrochemistry.

RAW MATERIALS

In this program, four different battery formulations are to be evaluated – these include a control along with three different carbon modified batteries. The carbon containing batteries consist of an acetylene black carbon, an activated carbon, and a combination of carbon black and a graphitic carbon. Batteries demonstrating the desired enhanced performance have been built in the past by East Penn Manufacturing for both the activated carbon and combination of carbon black and graphite. The acetylene black carbon is an electrically conductive material that, based upon theories within the literature, should have a similar beneficial effect. As it is unclear which characteristics of the carbon might be beneficial, a complete characterization of each material was performed.

Structural Analysis of Carbons

Physically, the acetylene black (Figure 6) and carbon black (Figure 7) are very similar. Both consist of agglomerations of extremely small particulate (approximately 20-30 nm in size), as illustrated below. The graphitic carbon (Figure 8) is very different than the carbon black and acetylene black materials, consisting of numerous platelets of graphite with a particle size on the order of tens of micron. The activated carbon (Figure 9) consisted of larger, blocky particles and has a glassy appearance to it (in terms of the fracture surfaces/edges of the particles).

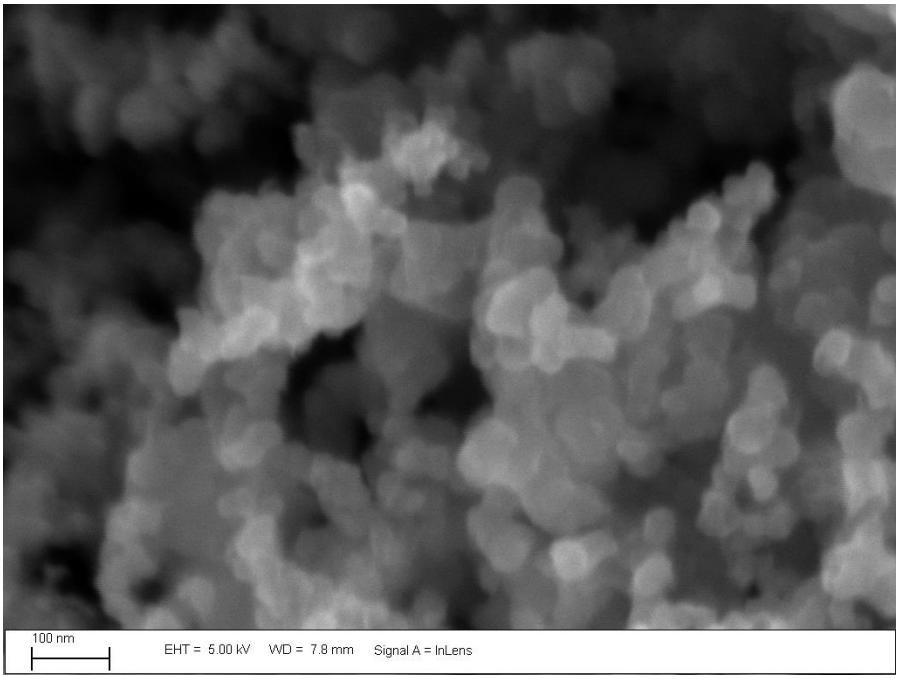

Figure 6: SEM image of the acetylene black material. The material consists of agglomerations of small (20-30nm) particles

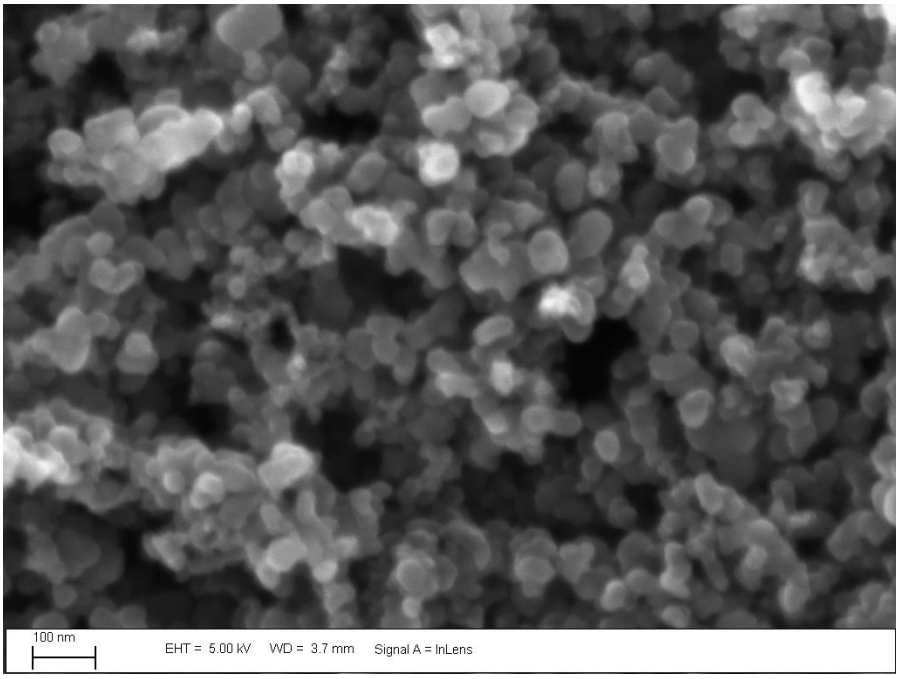

Figure 7: SEM image of the carbon black material. The material consists of agglomerations of small (20-30nm) particles, similar in appearance to the acetylene black.

Figure 8: SEM image of the natural graphitic material. The material consists of numerous plates of graphitic carbon, as expected for such materials.

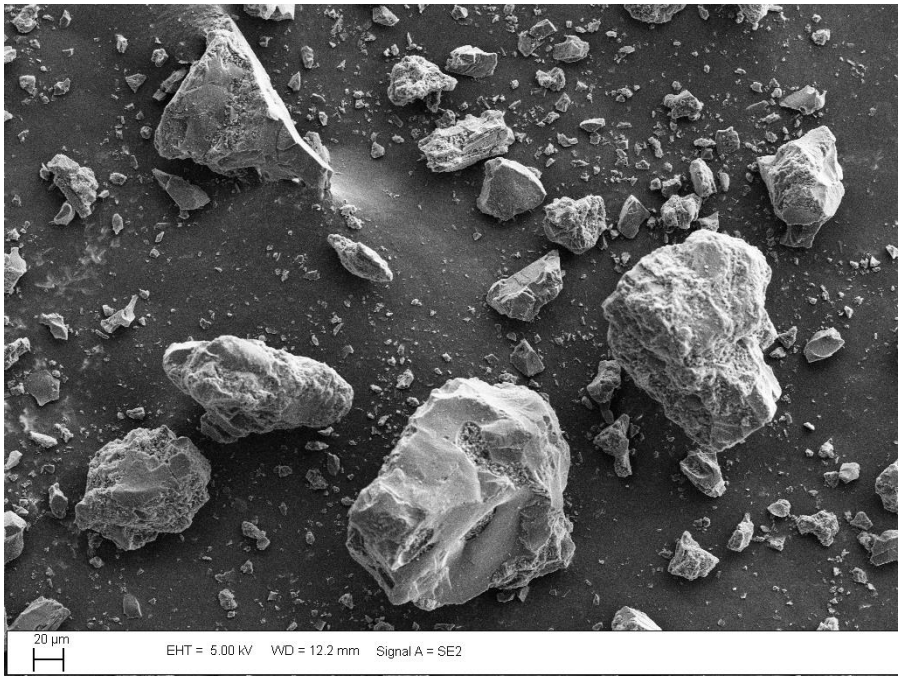

Figure 9: SEM image of the activated carbon material. This material consists of a variety of large and small particles, and has an amorphous appearance to it (based upon the fracture surfaces particularly visible on the larger particles).

X-ray diffraction was used to probe the crystalline structure of each of the materials (Figure 10). The graphitic carbon had well-ordered hexagonal graphite (type 2H) diffraction data, as anticipated for this highly crystalline material. The activated carbon exhibited a diffraction pattern consistent with amorphous material, further supporting the physical observation of a glassy-appearing material. The acetylene black and carbon black had diffraction patterns that were similar to graphite, with the main diffraction peak shifted to larger d-spacings (Table 1). The shift in spacings and considerable peak broadening suggest that they have a very fine crystallite size. Both of these materials exhibit evidence of a mixture of nano-crystalline as well as amorphous type peaks. This was more easily observed in the carbon black sample which had two distinctly different peak profiles (one sharper, one broader). The acetylene black peak profile fitting resolved two discrete peaks, but the broadness of the peaks made clear distinction of peak location and degree of peak broadening determination difficult.

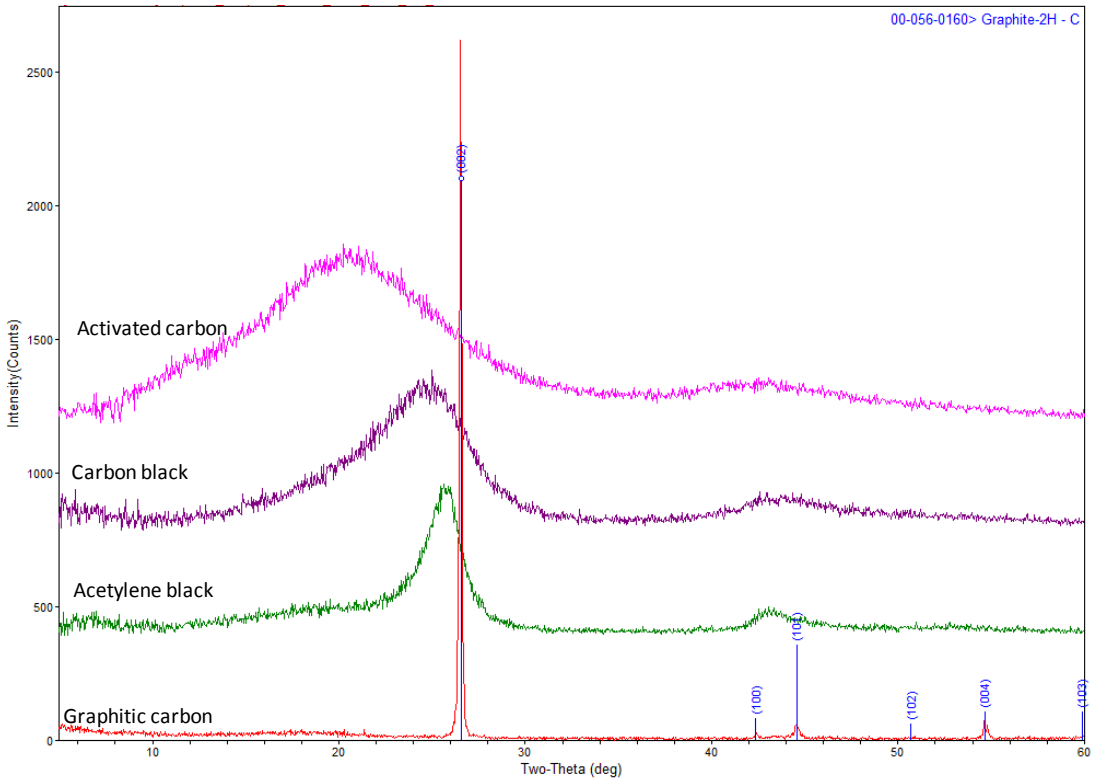

Figure 10: Comparison of the x-ray diffraction data from the four carbon materials, illustrating the crystalline structure (or lack thereof) for each material.

Table 1: Carbon Lattice Spacing and Degree of Crystallinity

Sample	Main peak - pseudo (002) peak					Broad peak – amorphous signature				
	2θ (º)	d-spacing (Å)	FWHM (º)	Xtal size* (Å)	Relative Peak Area	2θ (º)	d-spacing (Å)	FWHM (º)	Xtal size* (Å)	Relative Peak Area
Graphite	26.538(1)	3.3560(1)	0.095(2)	>1000	100	18.1(2)	4.9(1)	5.7(5)	14(2)	17.1
Acetylene Black	25.84(4)	3.45(1)	2.26(6)	37(2)	100	19.3(7)	4.6(3)	10.7(8)	8(2)	56.3
Carbon Black	24.8(1)	3.59(4)	5.3(1)	16(1)	100	19.7(6)	4.5(3)	6.6(6)	12(2)	35.8
Activated Carbon						20.5(1)	4.33(1)	11.3(2)	7(1)	100
*Crystallite size estimates are based on Scherer equation – values less than 10 Å strongly suggests amorphous characteristics										

Based upon the x-ray diffraction data, the degree of crystalline order of the four materials is ranked as follows (from most crystalline to least crystalline (amorphous))

1. Graphitic carbon
2. Acetylene black carbon
3. Carbon black
4. Activated carbon

In addition to the basic geometry and phase structure of the carbons, the Brunauer, Emmet, and Teller (BET) surface area (i.e., the specific surface area of the materials per unit mass of material determined via gas adsorption) was analyzed (Table 2). With one exception, the results are as one might predict from the shape/size of the individual particulate in each material.

Table 2: Raw Carbon BET Surface Areas

	Activated Carbon	Carbon Black	Acetylene Black	Graphitic Carbon
sample 1	2077.98 ± 7.93 m^2/g	74.21 ± 0.21 m^2/g	75.05 ± 0.46 m^2/g	6.55 ± 0.03 m^2/g
sample 2	2052.74 ± 9.17 m^2/g	73.22 ± 0.22 m^2/g	74.63 ± 0.42 m^2/g	7.30 ± 0.05 m^2/g
sample 3	2048.56 ± 6.51 m^2/g	73.72 ± 0.18 m^2/g	75.34 ± 0.44 m^2/g	6.66 ± 0.02 m^2/g

The carbon black and acetylene black, being similarly sized particles, are expected to have the same basic surface area per unit mass, as confirmed via BET measurements. The graphitic carbon, having larger particles/plates, would be expected to have a considerably lower surface area than the carbon black, and BET measurements demonstrated that there is nearly an order of magnitude difference. However, the activated carbon, which had the largest particles, would be expected to have (based upon their size) the smallest surface area, however, it has the largest – more than 25 times that of the carbon black. The reason for this large difference is the microscopic structure of the activated carbon. Being derived from wood, it is highly porous, and thus the actual surface area (which includes the walls of the pores) is vastly larger than the macroscopic surface area based solely on particle size. This porous nature is illustrated in Figure 11 below which, while it does not allow individual pores to be physically resolved, does illustrate the lattice-like structure of the material.

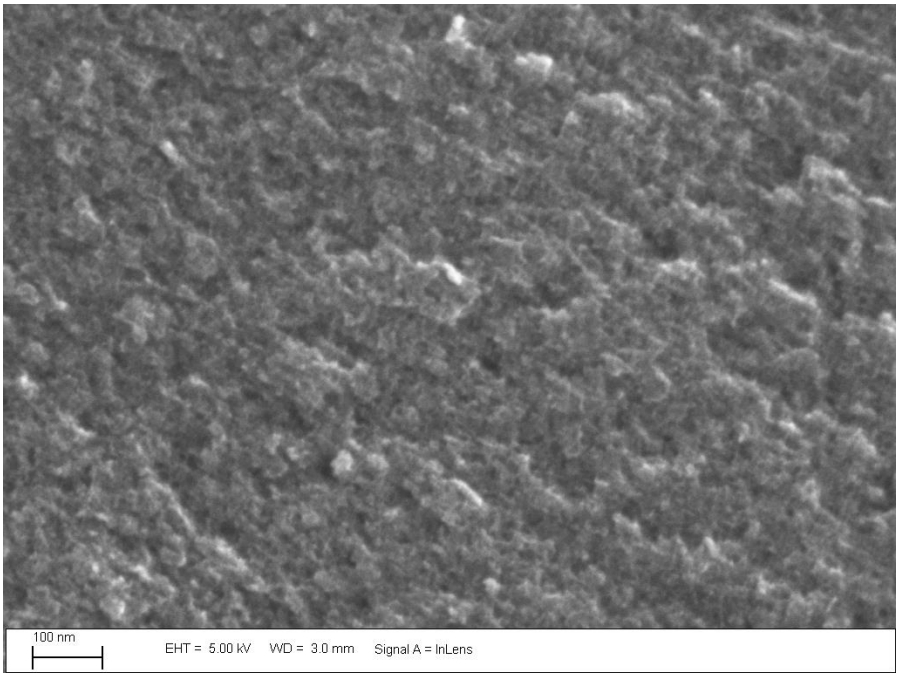

Figure 11: High resolution SEM image of the surface of an activated carbon particle. Being derived from wood, the material is extremely porous, and thus has a very high surface area per unit mass.

Based upon the literature, it was not clear which structure would be most effective as a battery addition. Clearly, the nature of the carbon surfaces (chemical reactivity and surface area) will be important if the

material is electrochemically active within the NAM, as suggested by Pavlov (Pavlov, Nikolov, & Rogachev, 2010). However, if the carbon instead acts to increase the electrical conductivity of the NAM, then the ability of the carbon particles to provide a conductive network may be more important, in which case smaller particulates such as the carbon black or acetylene black may be more beneficial.

Chemical Analysis of Carbons

In addition to the structure of the carbon additions, the nature of any soluble contaminant species which they might contribute to the electrolyte within the battery may have an impact on the performance of the system. Specifically, detrimental species such as iron may act to poison the electrochemical reactions which take place within the battery as it functions.

Samples of all four carbon materials were also analyzed for their acid soluble contaminant species, as well as the accompanying anions. The results of these experiments are presented below in Table 3 and Table 4. Each table entry represents the average and standard deviation obtained from three runs of each material. Acid soluble contaminants were extracted in 6N HCl and then analyzed via ICP-MS. Anions were extracted by sonicating the carbon specimens in water and then analyzing the leachate via ion chromatography.

Table 3: Acid Soluble Contaminants in Carbon Samples (ppm by weight)

	Al	B	Ba	Ce	Fe	K	La	Mg	Mn	Mo
Carbon Black	10.5 ± 0.6	--	--	--	6.24 ± 0.79	123 ± 8	2.48 ± 0.19	287 ± 12	0.57 ± 0.09	--
Acetylene Black	--	--	--	--	--	0.96 ± 1.07	--	--	--	--
Activated Carbon	28.3 ± 0.8	2.35 ± 1.21	1.03 ± 0.03	--	91.6 ± 5.8	13.4 ± 2.5	--	12.5 ± 0.3	1.83 ± 0.15	--
Graphite	--	--	--	0.85 ± 0.03	--	--	--	--	--	0.95 ± 0.08

	Na	Ni	Pb	Sr	Ti	Zn	Zr
Carbon Black	89.9 ± 5.7	--	--	--	0.51 ± 0.09	--	--
Acetylene Black	--	--	--	--	--	--	--
Activated Carbon	2450 ± 30	1.65 ± 0.62	--	1.04 ± 0.14	15.2 ± 0.7	2.54 ± 1.00	--
Graphite	--	--	2.96 ± 1.02	--	7.3 ± 0.31	--	3.04 ± 0.21

Table 4: Water Soluble Anions in Carbon Samples (ppm by weight)

	Sulfate	Nitrate	Phosphate	Chloride	Fluoride
Carbon Black	3920	trace	--	trace	trace
Acetylene Black	--	--	--	--	--
Activated Carbon	94.1	71.1	11929	--	--
Graphite	--	--	--	--	--

All of the observed values were in line with past data, and consistent with the type of material being analyzed. As expected, the acetylene black material was very clean, followed by the natural graphite. The activated carbon contained significant contaminants, including nearly 100ppm Fe.

AS-RECEIVED BATTERY PLATES

Four different battery formulations were evaluated in this study. These included a control along with three different carbon modified batteries. The carbon containing batteries consisted of a battery where the negative active mass contains either acetylene black carbon, activated carbon, or a combination of carbon black and graphitic carbon. The physical structure of the plates used to construct each battery type was assessed in both the as-pasted and formed condition. In addition, the baseline electrochemical properties of the different formulations have been assessed. Plates were evaluated both in the raw (i.e., as pasted and cured) and formed condition. Through the forming process, the as pasted material, which is a combination of lead oxide, lead sulfate, metallic lead, and various other additions (expanders, the carbon, etc.), is electrochemically transformed to predominantly metallic lead such that it can effectively function within the battery.

Cross Sectional Analysis of Negative Active Material

Samples of the raw and formed negative plates for each battery type were cross sectioned metallographically, and then evaluated within the SEM. The figures below contain representative images from each plate type. Several features were observed which were common to all of the plate types. These were generally related to the binder and other materials which make up the general formula for the negative active material. In some cases, such as with the acetylene black and carbon black, small regions were visible within the plate that were far more porous than the surrounding material. While the origin of these regions is unclear, they may be the result of large agglomerates of the two carbon materials which were visible when evaluating the carbon prior to being placed within the battery. In all cases, the carbon appeared to be well dispersed through the thickness of the plate. In addition, in the case of the activated carbon, a chemistry previously explored by East Penn Manufacturing, there is strong evidence that the carbon is itself electrochemically active, allowing for the formation of metallic lead throughout the material during the forming process.

A cross sectional view of a negative plate from a typical control cell is shown in Figure 12. Cylindrical/fibrous materials are the binder used in the standard formulation of the negative active material, and can be seen in the carbon containing cells as well. Cross sections of raw and formed plates from an activated carbon containing battery are shown in Figure 13. The activated carbon particles are large, and readily visible within the structure. No agglomeration was observed. In Figure 14, an image of a single activated carbon particle is shown, along with an EDS map of Pb. Metallic Pb is clearly visible throughout the fissures within the carbon particle, strongly suggesting that this carbon species is electrochemically active.

Cross sections of the acetylene black containing plates are shown in Figure 15. Carbon particles are well distributed and not generally visible within the structure due to their very small size (Figure 6). There are some regions which appeared more porous, which may be the result of large agglomerates of carbon particles, as illustrated previously for the carbon itself prior to incorporation in the negative active material. Finally, cross sections of the carbon black plus graphite containing plates are presented in Figure 16. Both materials appear to be well dispersed through the plate, but only the graphitic carbon is visible. As with the acetylene black material, regions which appeared more porous are visible throughout the plate, potentially due to large agglomerates of the carbon black material.

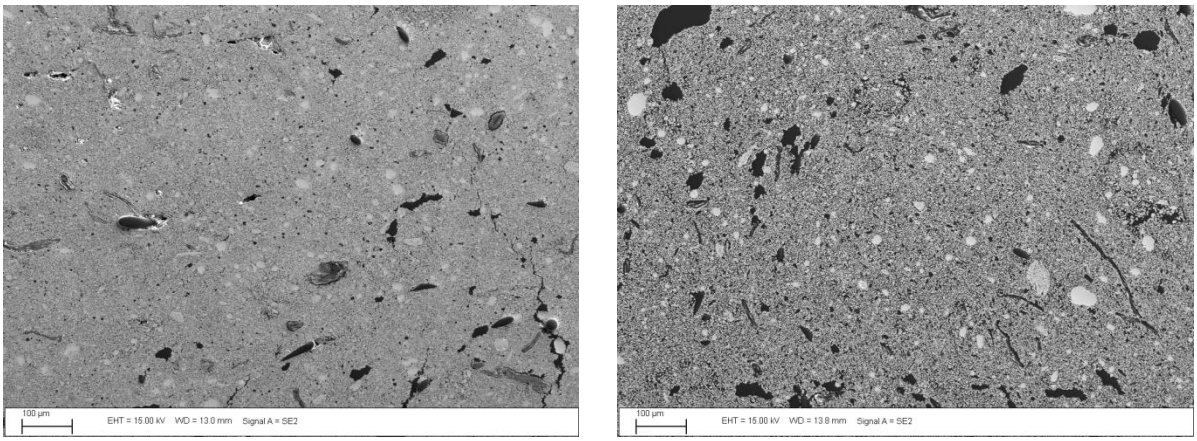

Figure 12: Control battery – raw (left side) and formed (right side).

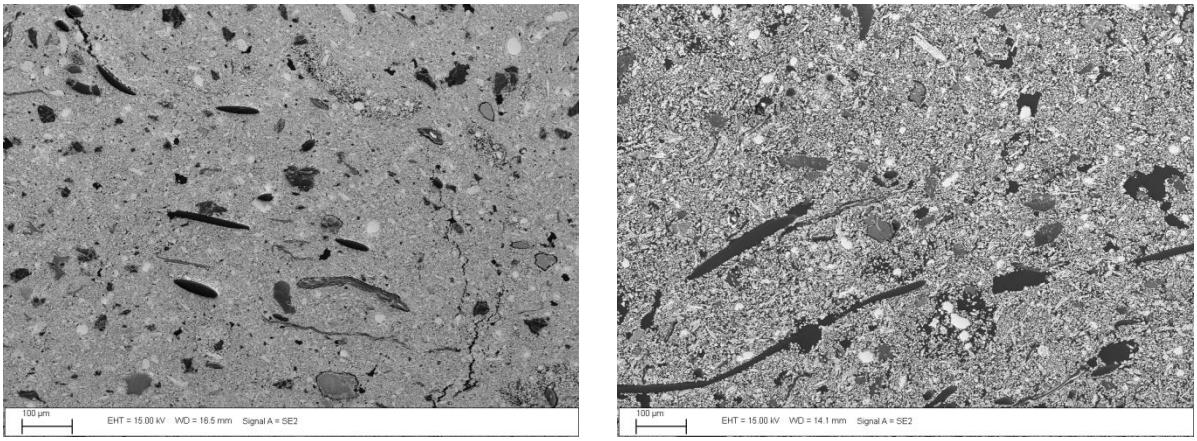

Figure 13: Activated carbon containing battery – raw (left side) and formed (right side). Carbon particles are well dispersed and clearly visible in the matrix as large, blocky particles (see Figure 14).

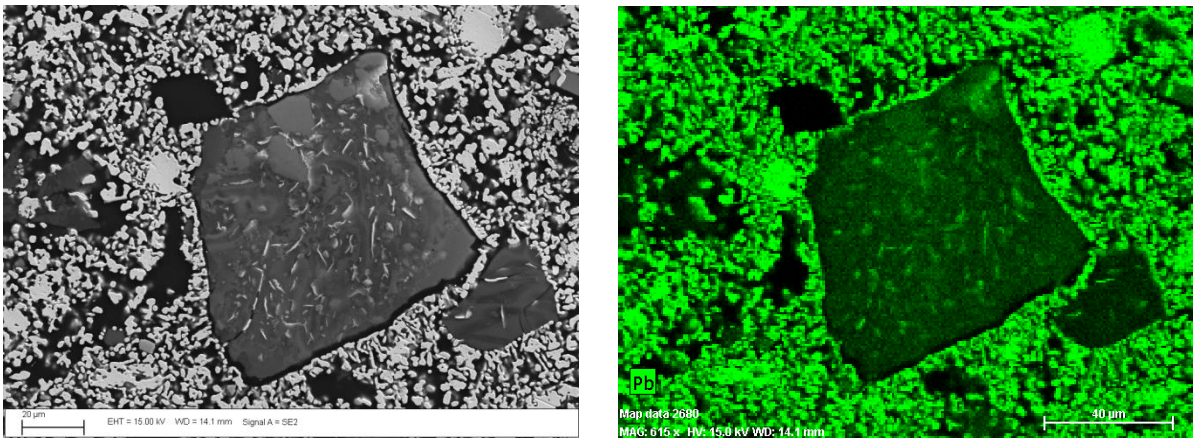

Figure 14: Activated carbon particle from a formed plate, illustrating that metallic lead can be found throughout the fissures/pores within the carbon. Image on right side is a compositional map, with green indicating presence of lead, confirming that the material within the carbon particle is indeed lead.

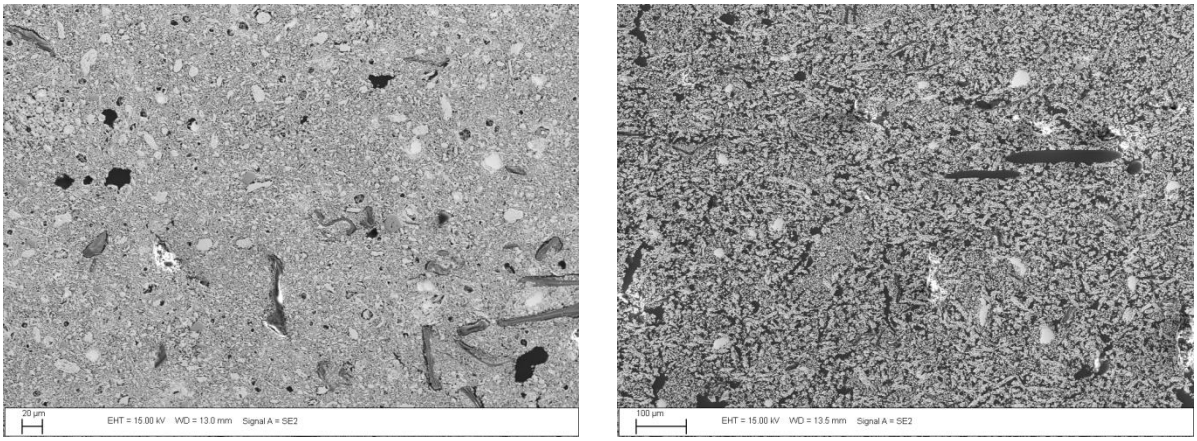

Figure 15: Acetylene black containing battery plate – raw (left side) and formed (right side). Carbon particles are well distributed (i.e., no significant agglomeration)) and not generally visible within the structure.

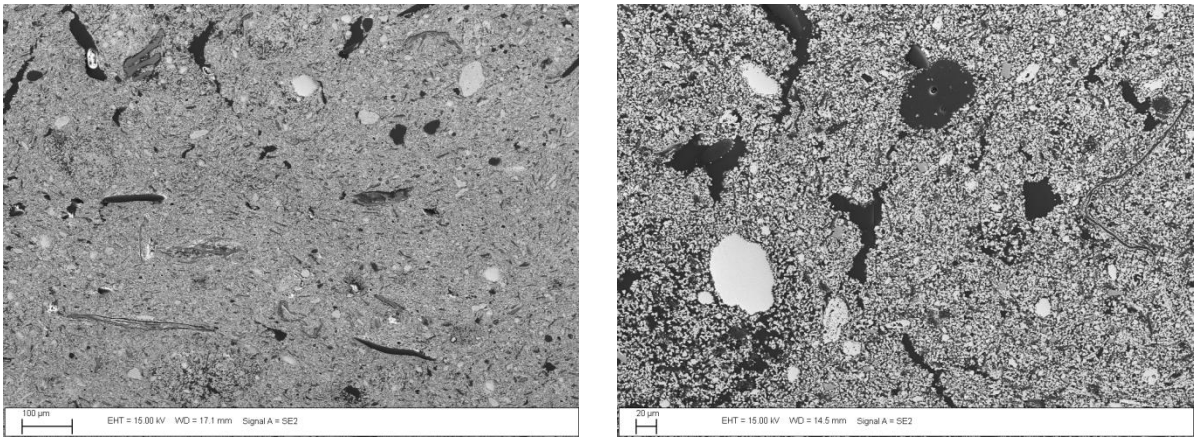

Figure 16: Carbon black and graphitic carbon containing plates – raw (left side) and formed (right side). Both materials appear to be well dispersed through the plate (i.e., no significant agglomeration), but only the graphitic carbon is visible (plate-like particles).

Microscopic Plate Porosity

In order to effectively utilize the entire negative active material within the plate, the battery relies on pores within its structure to allow solution to penetrate through the thickness of the plate and maximize the surface area of metallic lead available for reaction. Mercury porosimetry was utilized to explore the overall porosity of each carbon containing negative plate as well as the control. As can be seen in Table 5 below, the degree of porosity was similar when comparing the various materials.

In addition to the overall degree of porosity, the distribution of pore sizes can also be extracted from the mercury porosimetry data. As can be seen in Figure 17, in all cases, both the overall pore volume and the pore-size increases as the plates are formed. Comparing the different materials, the distribution of pore sizes is shifted to larger values when the carbon is present. This is particularly true for the plates containing activated carbon or a combination of activated carbon and carbon black. It is likely that the

large particle size found with the activated carbon and the graphitic carbon result in an increase in the typical pore size, whereas for the acetylene black containing plates, the carbon particles do not result in a modification of the pore structure of the negative active material. The pore distribution was also be monitored as a function of time as the batteries were cycled.

Table 5: Total Porosity of Raw and Formed Negative Plates

	% Porosity	
	Raw	**Formed**
Control	39.7	59.2
Acetylene black	44.8	55.8
Graphitic carbon + carbon black	45.7	59.5
Activated carbon	37.1	55.8

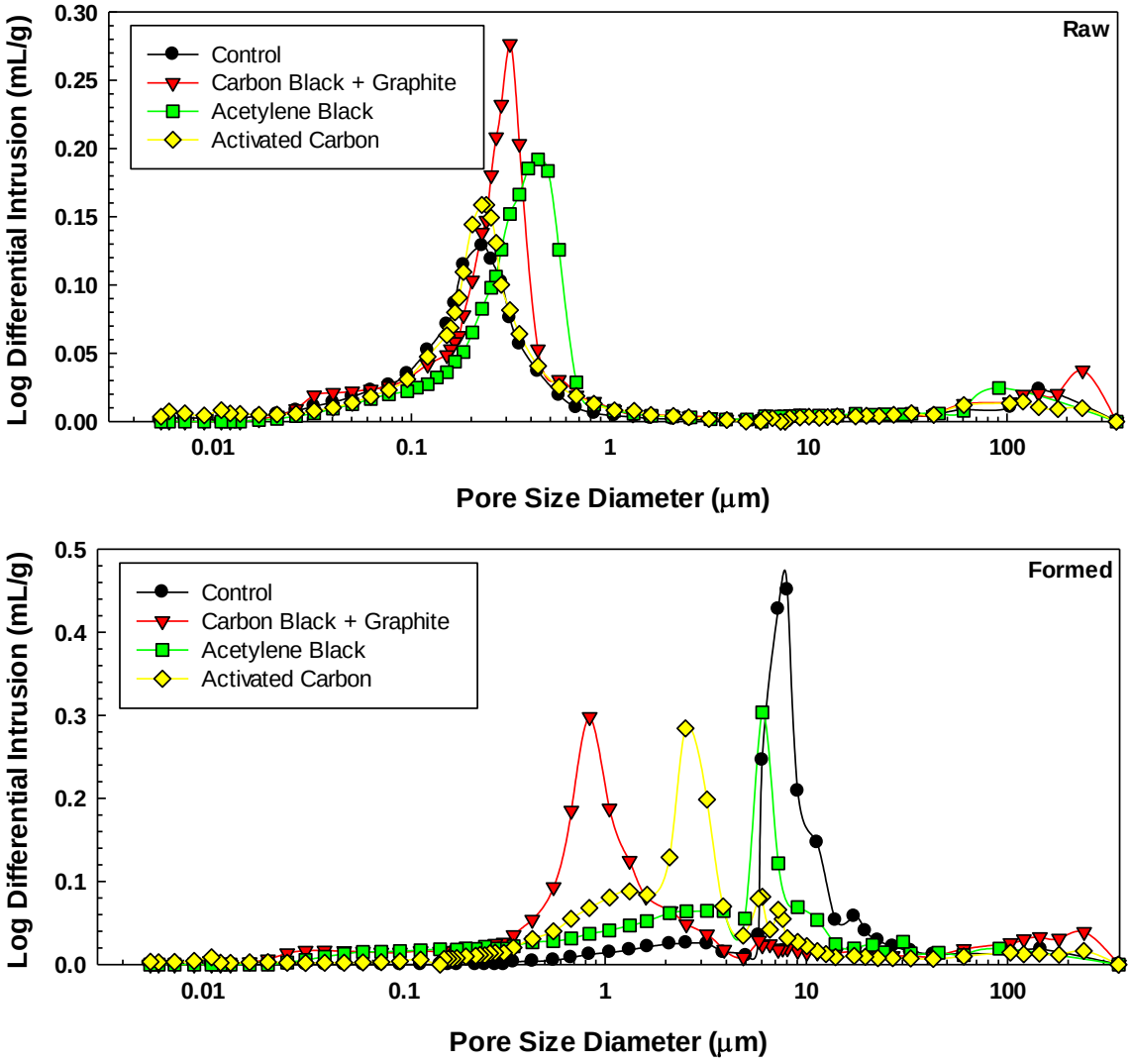

Figure 17: Differential intrusion (of Hg) as a function of pore size diameter, illustrating the distribution of pores found in each formulation in the raw and formed state.

BASELINE ELECTROCHEMICAL PERFORMANCE DATA

The baseline electrochemical performance of each battery type was evaluated. This information will form the initial data point to which the batteries will be compared as they are cycled. The batteries themselves are based upon an existing case design produced by East Penn Manufacturing. The plate count within each cell was reduced such that the overall capacity would be on the order of 10 Ah. As a result, each cell contained a total of 5 plates – 3 negative plates, and 2 positive plates. For all structural analyses, only the center negative plate was evaluated in an effort to avoid potential complications due to the position of the plate relative to the edge of the stack. While the entire 6 cell battery was populated with positive and negative plates, only a single cell was filled with electrolyte and activated. As such, all of the electrochemical results are reported for a single cell, rather than multiple cells in series.

The open circuit potential and internal impedance of each battery was measured. As illustrated in Table 6, the open circuit voltage was nominally identical for all of the cells. Since the basic electrochemical reactions which occur within a VRLA battery remain unchanged by the addition of carbon, this result was expected. The internal impedance of the batteries was also measured, and was also nominally identical for the four battery types.

Table 6: Baseline Electrochemical Properties of Control and Carbon Containing Cells

	V_{oc} (V)	R (micro-ohm)
Control	2.147 ± 0.002	1997 ± 30
Activated Carbon	2.158 ± 0.003	2038 ± 36
Acetylene Carbon	2.141 ± 0.008	2015 ± 36
Carbon Black + Graphite	2.146 ± 0.005	2114 ± 20

A charging protocol was developed to assess the initial capacity of the different batteries. Each battery (single cell) was charged at 2.3 V (with a maximum current equal to the 1C rate) until the charging current fell to below 75 mA, then allowed to stand at open circuit for one hour. Next, the cell was discharged fully at a 1C rate to a final voltage of 1.75 V, and the total charge passed during the discharge process was recorded. After standing for an hour at open circuit, the cell was then recharged to 108% of the previously recorded discharge capacity (with the maximum current clamped at the 1C rate). Finally, after another hour at open circuit, each cell was discharged at a 1C rate to 1.75 V, and the total charge passed during the discharge process recorded. This second discharge capacity was logged as the cell capacity. The distribution of capacities, along with the average capacity and standard deviation are presented in Figure 18 and Table 7.

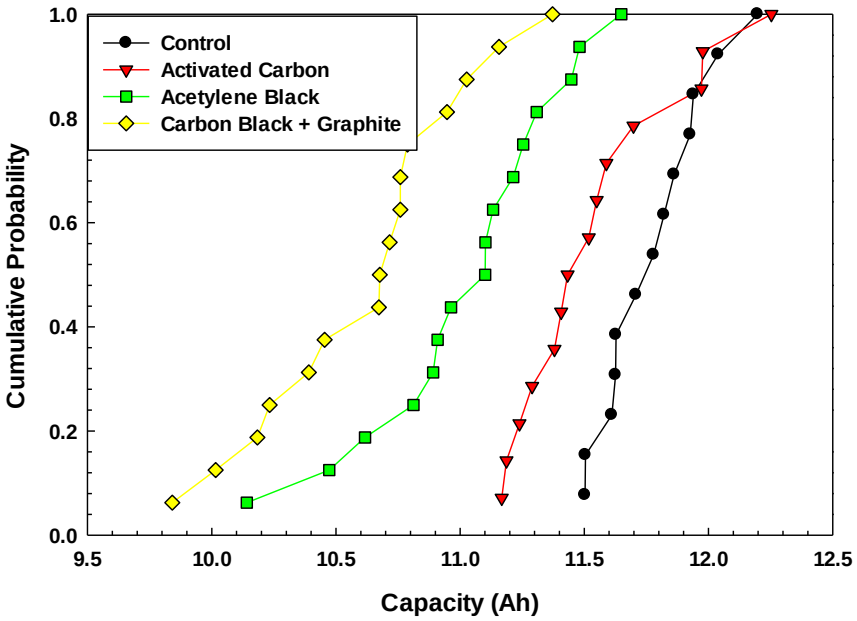

Figure 18: Capacity distribution for each of the battery types evaluated. Note that the "battery" consists of a single cell.

Table 7: Average Capacity of Control and Carbon Containing Cells

	Capacity (Ah)
Control	11.78 ± 0.21
Activated Carbon	11.55 ± 0.33
Acetylene Black	11.03 ± 0.39
Carbon Black + Graphite	10.63 ± 0.42

As expected, the control cells, which are based upon a highly optimized production process, have the tightest distribution of capacities. The carbon containing batteries had a more substantial distribution, as well as a lower overall capacity. The reduced initial capacity for the carbon containing batteries was not unexpected as the carbon has displaced some of the active material (i.e., a certain percentage of the negative active material has been replaced with carbon), resulting in a lower quantity of material available for reaction within the cell. It should be noted, though, that these batteries typically increase in capacity with cycling, as has been noted in past work performed at Sandia as well as other laboratories.

Once the capacities were determined utilizing the procedure described above, the batteries were then recharged following the same procedure (i.e., charge to 108% of the previously measured discharge capacity). Three examples of each battery type were then set aside to evaluate the degree of self-discharge that occurs over a 6 month period.

The float current for each battery type was measured at a series of five voltages. Three examples of each material were evaluated. Float current measurements were carried out by first charging each battery at a fixed potential of 2.45 V for 24 h. The batteries were then allowed to rest for 48 h. Next, each battery was held at a fixed potential of 2.27 V for ten days, and the final current (the float current at that voltage) measured. This process was repeated by holding each battery at a potential of 2.30 V, 2.35 V, 2.40 V and

2.45 V for periods of 72 h, 24 h, 12 h and 6 h respectively. The resulting float currents are presented in Figure 19.

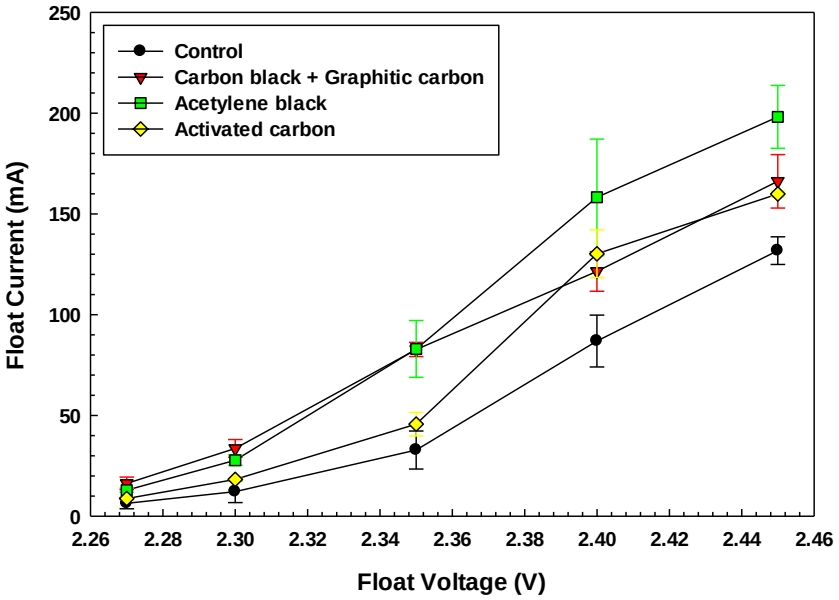

Figure 19: Float current as a function of applied potential for each of the battery types evaluated. In all cases, the float current is increased by the presence of carbon when compared to the control.

The float current is a measure of the rate of reactions which occur during the overcharge of the battery (i.e., each cell is being held at a potential greater than the open circuit potential of a fully charged cell). These reactions include oxygen evolution and potentially grid corrosion at the positive electrode, along with hydrogen evolution (and oxygen reduction) at the negative plate. In all cases, the float current was observed to increase when carbon was added to the negative active material. While the precise explanation for this increase has not yet been determined, it would be reasonable to assume that the increase was the result of more effective water reduction on the carbon surface.

HPPC testing

The Hybrid Pulse Power Characterization (HPPC) test, as defined in the "FreedomCAR Battery Test Manual" (DOE, 2003) was performed for each of the four battery types under evaluation in this study. As stated in the aforementioned report, the goal of this test is to establish the ability of the battery to deliver power or accept charge as a function of the state of charge of the battery over the useable range of voltages for the battery. The test was performed on new/untested examples of each battery, and repeated on batteries which were cycled in an effort to observe the degradation of battery performance over time.

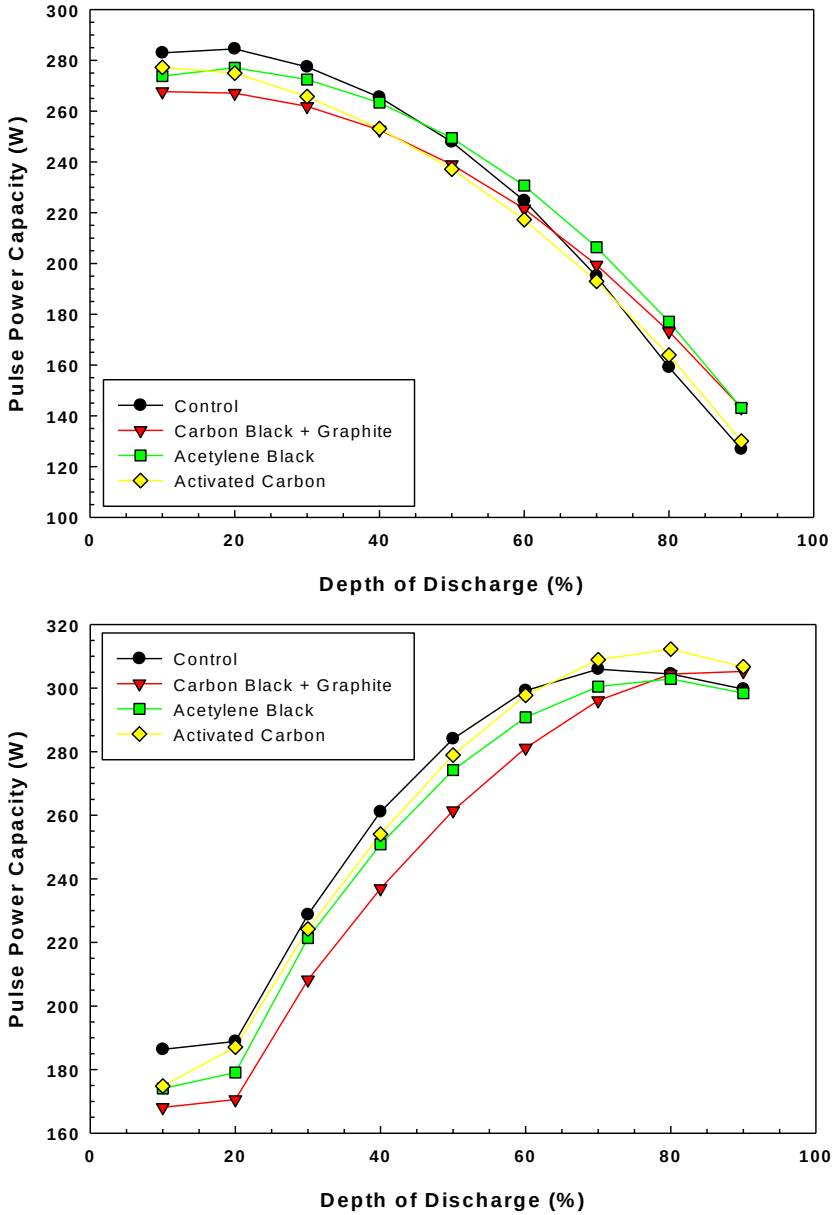

Figure 20: HPPC discharge (upper graph) and charge (lower graph) capacities for fresh examples of each battery type. While the graphs indicate some differentiation between batteries, as only a single example of each type has been evaluated, it is difficult to attach statistical significance to any of the observed differences.

Looking at the data in Figure 20, it can be seen that all four battery types behave similarly. While some differentiation can be seen, at this time only a single example of each battery has been run. As a result, the degree of variability associated with each battery type is not known, and it is not possible to state that the differences seen in the figure are statistically significant.

6 Month Self Discharge

All batteries will self-discharge over time. In order to evaluate the rate at which the carbon modified cells would self-discharge, a series of batteries of each type was charged to full capacity, then allowed to sit idle for six months, after which the capacity was measured again. The concern with the carbon modified cells was that the additional electrochemically active surface area added by the carbon would provide additional cathodic surface area which would then support discharge of the negative active material. As illustrated in the Figure 21, this appears to have proven to be true.

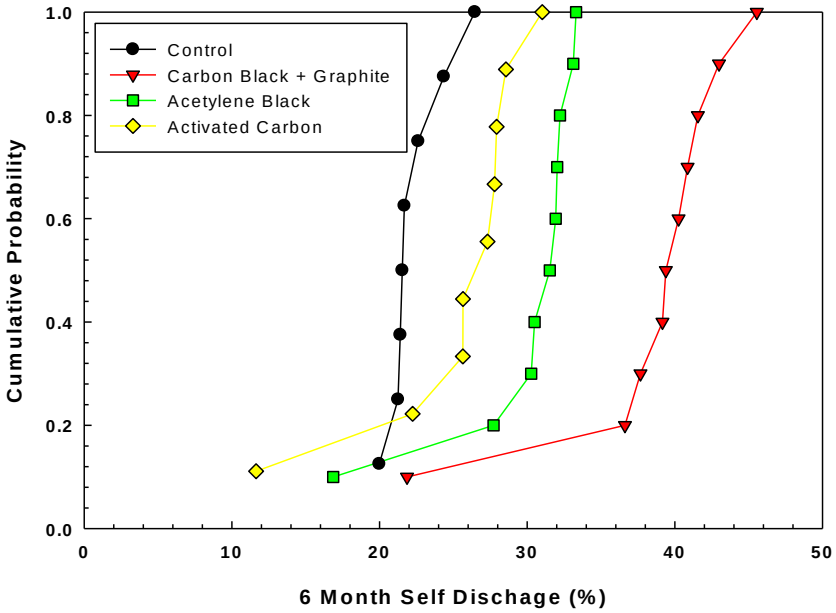

Figure 21: Self discharge rate for the control and carbon containing batteries. As illustrated in the figure, all of the carbon containing batteries had a significantly higher degree of self-discharge

All of the carbon containing batteries exhibited an elevated rate of self-discharge. A likely explanation for this effect is that the carbon, which has been demonstrated to be electrochemically active within the plate, is serving as a cathode, driving dissolution of the lead within the negative plate, resulting in an increased loss of capacity with time.

CYCLE TESTING

Examples of each battery type were subjected to a high-rate partial-state-of-charge (HRPSoC) cycle profile designed to simulate the ancillary regulation services of a utility and a wind farm energy smoothing application (Hund, Clark, & Baca, 2008). The HRPSoC cycle test uses a 10% discharge cycle at the 1C1 to 4C1 (C1 = 1 hr Ah capacity) discharge and charge rates at near 50% state of charge (SOC) to provide the maximum power and energy performance. After 1000 cycles, all four battery types behaved nominally identically. As illustrated below, upon dissection there were some differences observed. After 10,000 cycles, the different compositions began to distinguish themselves. A capacity loss was evident in the control, acetylene black, and activated carbon batteries. The carbon black + graphite cell, however, exhibited a slight increase in capacity at this point. As the batteries continued to cycle, a control cell failed at 11,292 cycles. Batteries at each stopping point (1k and 10k cycles) were destructively evaluated to observe the structure of the plates as the batteries were aged.

Once removed from the cycling tests, the batteries were disassembled in a glove box with a nitrogen atmosphere. Plates were then rinsed thoroughly in deionized water and allowed to dry. Once dried, samples were taken from each plate, as illustrated in Figure 22, for a variety of analytical techniques.

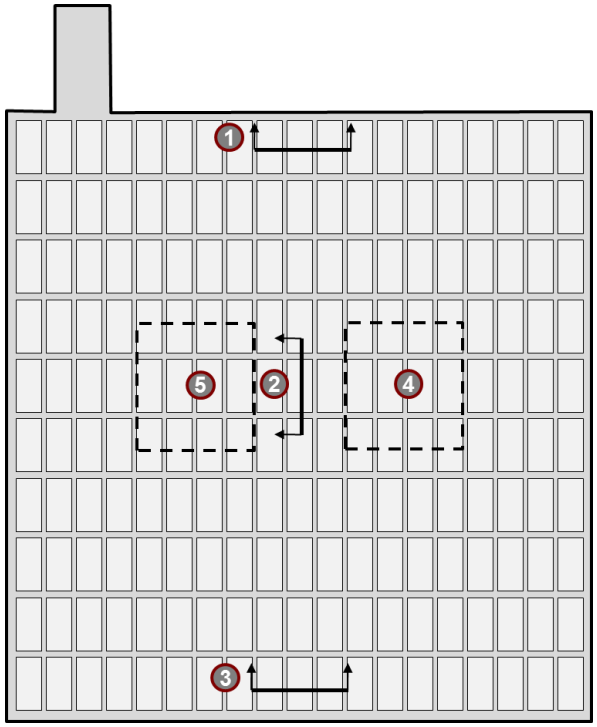

Figure 22: Location of cross sections taken for analytical evaluation of each plate. Locations 1, 2, and 3 were used for SEM analysis of the structure of the active material. Region 4 was taken for Hg porosimetry and region 5 for BET surface area.

Mercury porosimetry was again used to evaluate the overall degree of porosity as well as the distribution of pore sizes within the plate. Samples were taken from the center of the plate for this analysis. It should be stressed that at the present time, only a single example of each battery has been evaluated at each stopping point, and as such the data should be used for qualitative comparisons, rather than a conclusive quantitative evaluation of the plates. In Table 8, the overall pore volume can be seen for each battery type in the initial (as formed), after 1000 cycles, and after 10,000 cycles. The overall pore volume appears to

be trending downwards for the activated carbon and acetylene black containing plates, but is relatively constant for the control and carbon black + graphite cell.

Table 8: Total Porosity for Each Battery Type after 1k and 10k Cycles

	% Porosity		
	Initial (Formed)	1k Cycles	10k Cycles
Control	59.2	57.4	61.1
Activated Carbon	55.8	47.3	48.0
Acetylene Black	55.8	53.6	49.0
Carbon Black + Graphite	59.5	55.7	56.8

In addition to the overall pore volume, the distribution of pore sizes within the plate was also determined. In
Figure 23, the distribution of pore sizes after 1000 and 10,000 cycles is illustrated (data for the raw and as-formed plates is presented above in the summary for the third quarter). After 1000 cycles, all of the carbon containing batteries had a distribution of pores in the 1 to 2 micron range, while the control had a portion around 3 microns and a large quantity closer to 7.5 microns. As the batteries continued to cycle to 10k cycles, the control cell lost the distribution of small pores, and was composed of pores from 7 to 10 microns in size. The cell containing the activated carbon behaved similarly, with the majority of the pores being in the 7 to 10 micron range. Both the carbon black + graphite cell and the acetylene black cells, however, remained essentially unchanged from 1000 cycles, with their distributions centered about 1 to 2 microns.

In addition to measuring porosity, negative plates for each formulation were cross sectioned and their structure evaluated. Furthermore, the distribution of lead sulfate crystals within the structure was also evaluated. A technique developed by B. McKenzie at Sandia was utilized to evaluate the lead sulfate distribution. In this technique, a Zeiss VPSE (Variable Pressure Secondary Electron) detector was used to image the features in the image that light up via cathodoluminescence. The detector is simply a light detector. As such, the VPSE detector was simply imaging the light given off by a luminescent material ($PbSO_4$) in the sample when it is impacted with the electron beam. This technique offers significant advantages over x-ray fluorescence in terms of the spatial resolution which is provided.

Cross sections were taken at the top, center, and bottom of each plate from batteries which had been returned to a 100% state of charge. The results after 1,000 cycles are illustrated in Figure 24. In the control cell, the sample possessed a globular structure similar to that seen in the as-formed plate. Lead sulfate crystals were distributed throughout the plate, with a thin layer beginning to form on the surface of the plate, suggesting the beginning of hard sulfation. The carbon containing cells had markedly less lead sulfate present within each plate, and in no cases was a layer visible on the surface of the plate. The plate containing carbon black + graphite had a different morphology than the others, with lead sulfate visible in the center of the plate, while a layer on the surface of the plate approximately 100-150 microns deep was completely clear of lead sulfate.

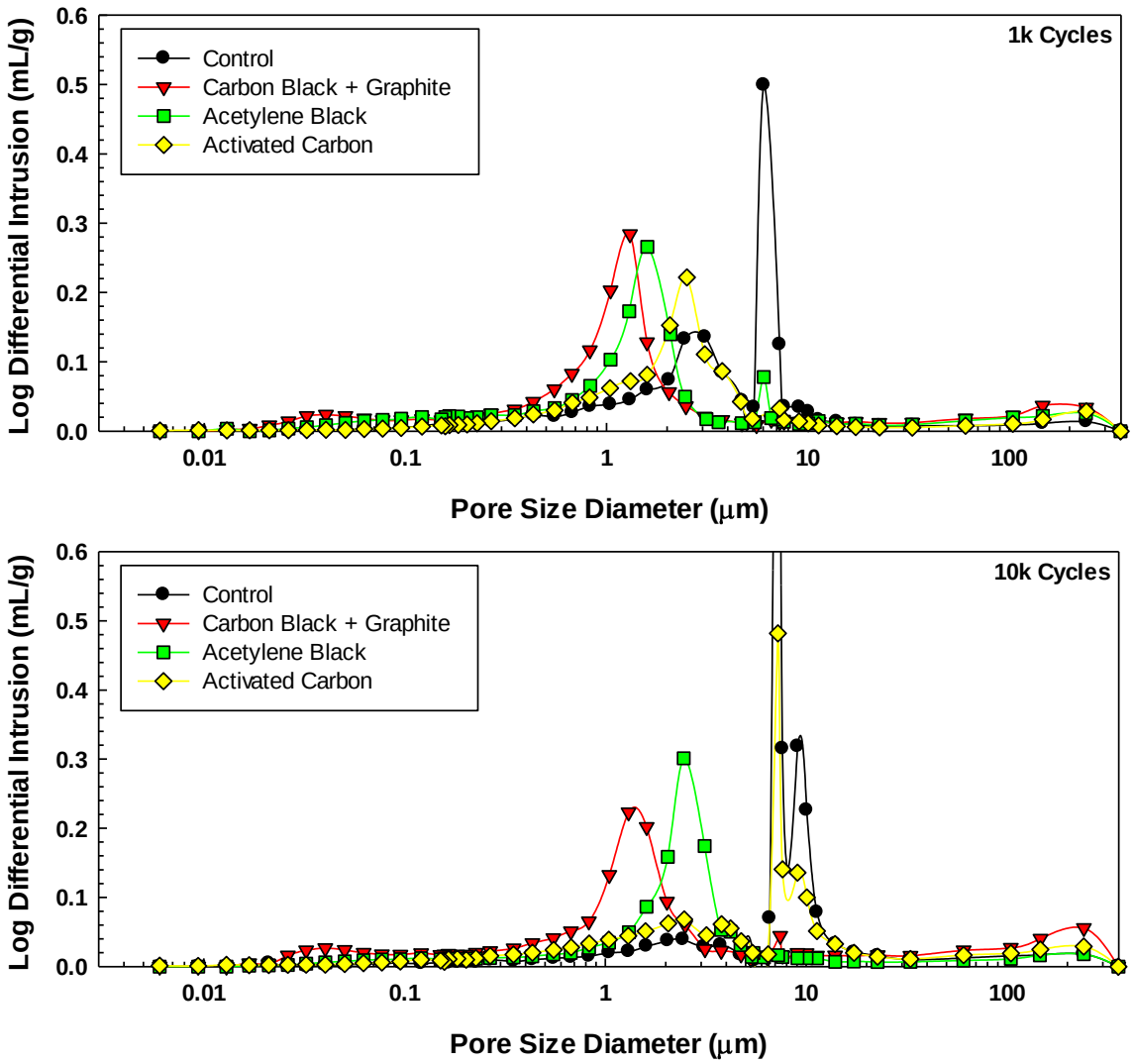

Figure 23: Intrusion rate as a function of pore size diameter, illustrating the distribution of pores found in each formulation after 1000 cycles (upper graph) and 10,000 cycles (lower graph).

After 10,000 cycles there were a number of marked differences between the four battery types (Figure 25). The control battery, which was within several thousand cycles of failure (based upon the single control battery tested to failure), had significant hard sulfation present on the surface of the electrode. As discussed previously, hard sulfation is promoted by the HRPSoC cycling to which these batteries are being subjected, and is the formation of a layer of lead sulfate on the electrode surface which is not be electrochemically reduced during the charging process. The activated carbon cell also had signs of hard sulfation, though not as severe as the control. In addition, the lead sulfate/hard sulfation appeared to be forming primarily in regions where a carbon particle was in close proximity to the electrode surface. Comparing this to the observations made via mercury porosimetry, it can be speculated that the lead sulfate is beginning to plug the smaller pores, which were possibly associated with the carbon particles. The plate containing acetylene black carbon was markedly different than the other batteries in terms of its physical structure, which appeared dendritic in nature. The plate was also completely clear of lead sulfate. Finally, the carbon black + graphite looked nominally identical to the 1000 cycle plate, with lead sulfate visible in the center of the plate, while a layer on the surface of the plate approximately 100-150 microns deep was completely clear of lead sulfate

Cells were then cycled to failure. As seen in Figure 26, the number of cycles to failure varied considerably within all of the battery types. Looking at the mean cycles to failure, the carbon black plus graphite containing cells had the longest cycle life, followed by the acetylene black, then the activated carbon, and finally the control cells. The average cycle life of the best carbon containing battery was approximately two and a half times that of the control cells. While the control cells had the tightest distribution, there was still considerable scatter, ranging from 11,294 cycles to 27,547 cycles. The carbon black plus graphite containing cells ranged from 31,373 to 60,121 cycles. The acetylene black from 23,862 to 58,435 cycles, and the activated carbon from 14,239 to 34,826 cycles. As such it does not appear that the scatter was due to incomplete optimization of the battery production process (for the carbon containing cells). By incorporating recovery charges each time the battery "failed" (i.e., each time its capacity fell below 80% of the initial capacity), the cycle life of all compositions was increased substantially, by a factor of two or more when compared to the average cycle life of that cell type.

Analysis of the batteries at failure did not reveal a clear, consistent "smoking gun" in terms of features that might have contributed to the loss of capacity. Structurally, cycling to failure resulted in an increased amount of what was observed at 10,000 cycles. In most of the carbon containing plates, and in particular for the carbon-black containing plates (both the carbon black and acetylene black) a sizeable population of large (tens of microns across and hundreds of microns long) voids became more prominent. The degree of sulfation was again very variable, ranging from almost complete, through the entire thickness of the active material, to cases where almost no sulfation was visible. The latter was observed primarily in carbon black containing cells.

An analysis of the BET surface area was performed for samples from each battery type at failure, as well as (with the exception of the activated carbon) after failure following multiple recovery charges. As illustrated in Figure 27, no change in the overall surface area of the negative active material was observed for the control, acetylene black, or carbon black plus graphite cells over their cycle life, including when recovery charges were used. The activated carbon containing cells, however, in addition to having a considerably larger surface area, saw that surface area decreased consistently over their cycle life (Figure 28). This latter observation was likely due to plugging of the microscopic porosity within the activated carbon particles over time.

Mercury porosimetry was again used to evaluate the pore structure within the negative plates. At failure (Figure 29), the pore distribution appeared to be similar for all four battery compositions. The majority of the pores were approximately 1 micron in diameter. In addition, a sizeable fraction of larger pores (100 microns and greater) was evident, particularly for the acetylene black containing plate, consistent with the observations made during the cross sectional analysis. The overall percentage of porosity is presented in Table 9. Comparing to the results from earlier in their cycle life (Table 8), all of the battery compositions lost a considerable fraction of their porosity between 10,000 cycles and the end of life. The most significant decrease was observed for the activated carbon containing cell, consistent with the considerable loss in BET surface area (Figure 28)

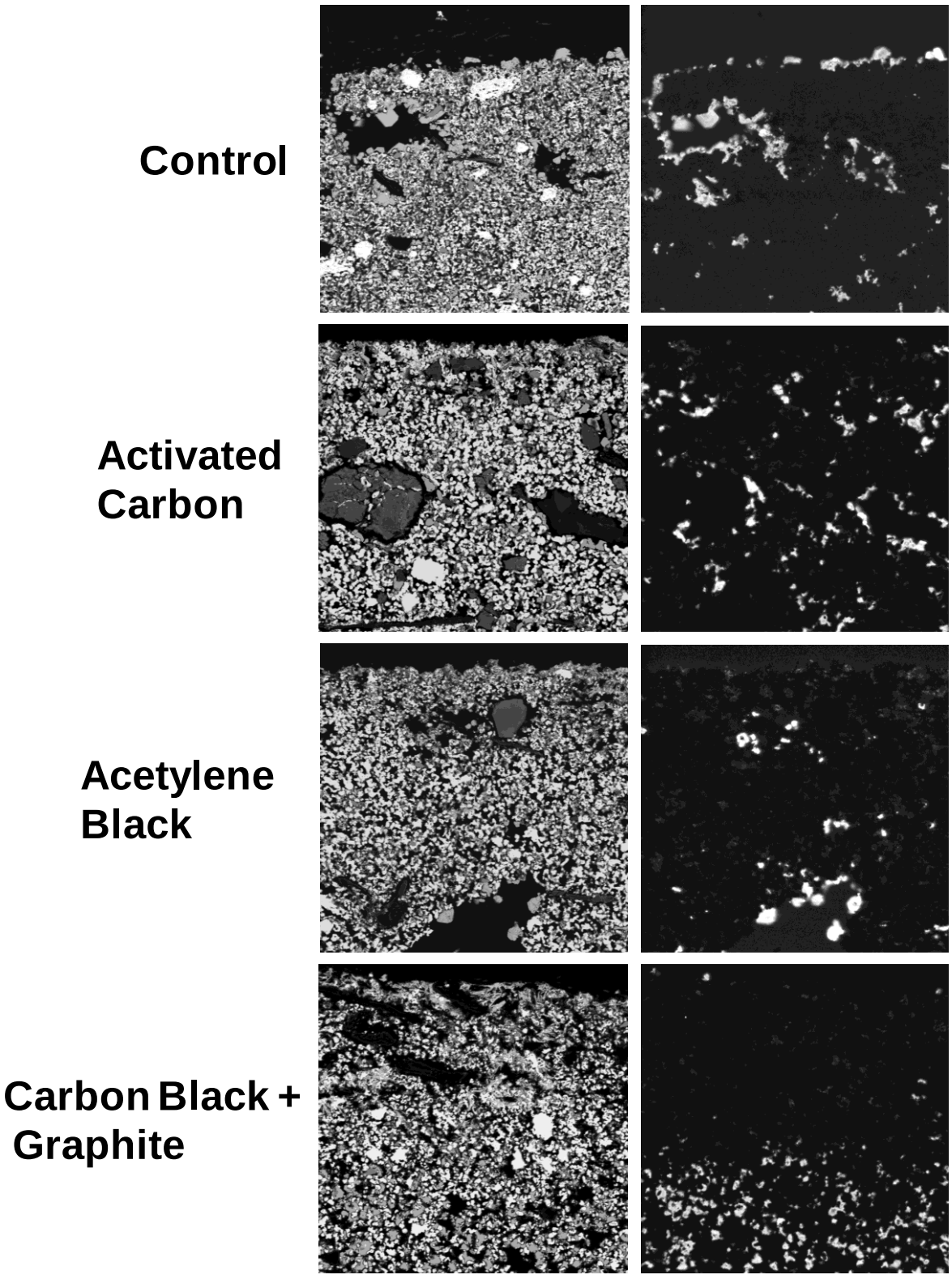

Figure 24: Representative cross sections from each battery type after 1000 cycles. Left image is a backscattered electron SEM image, while the right image is a cathodoluminescence image of the same location showing lead sulfate. Field of view for all images is approximately 264 µm.

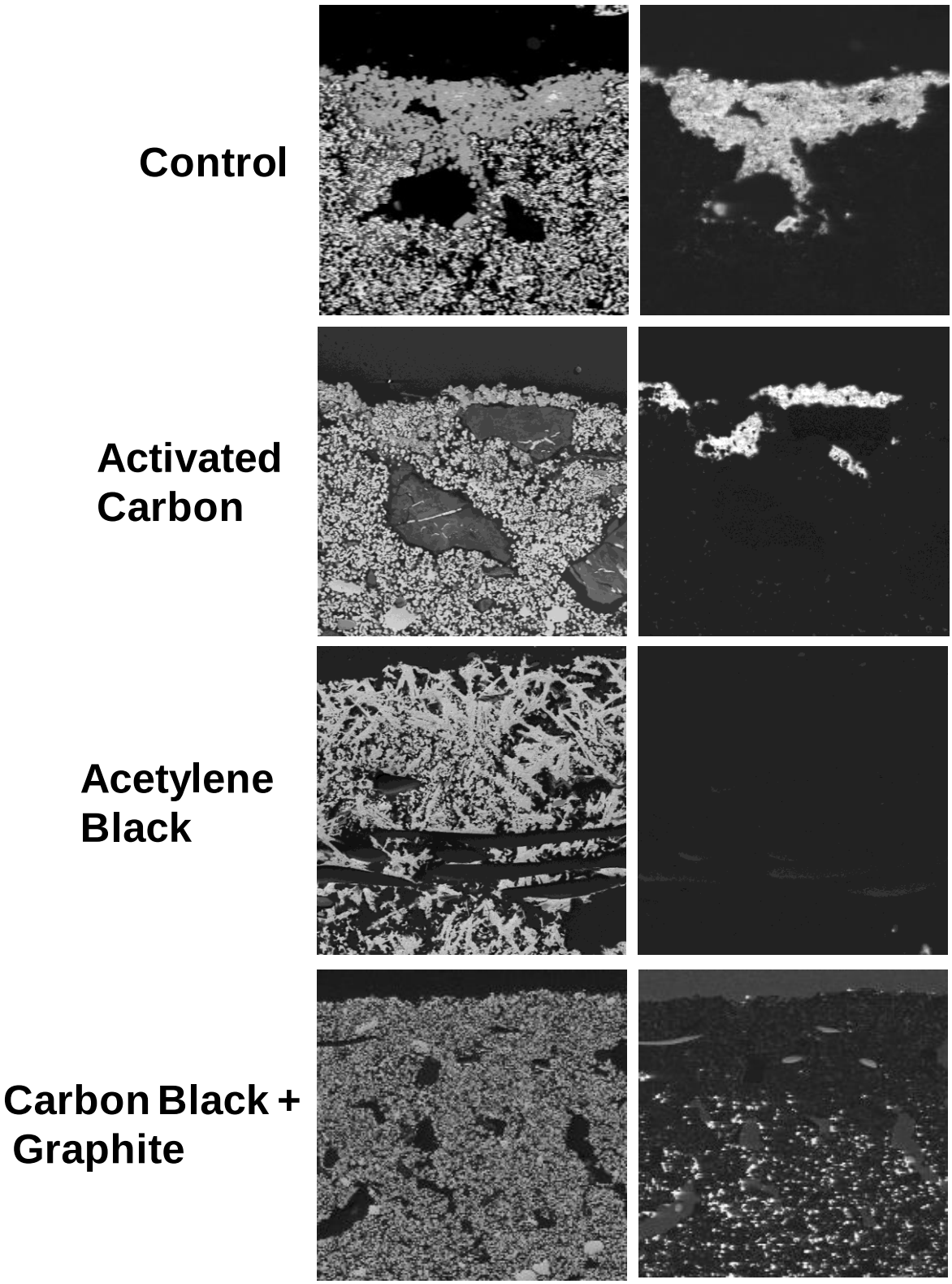

Figure 25: Representative cross sections from each battery type after 10,000 cycles. Left image is a backscattered electron SEM image, while the right image is a cathodoluminescence image of the same location showing lead sulfate. Field of view for all images is approximately 264 µm for all but the last image, where it is 633 µm.

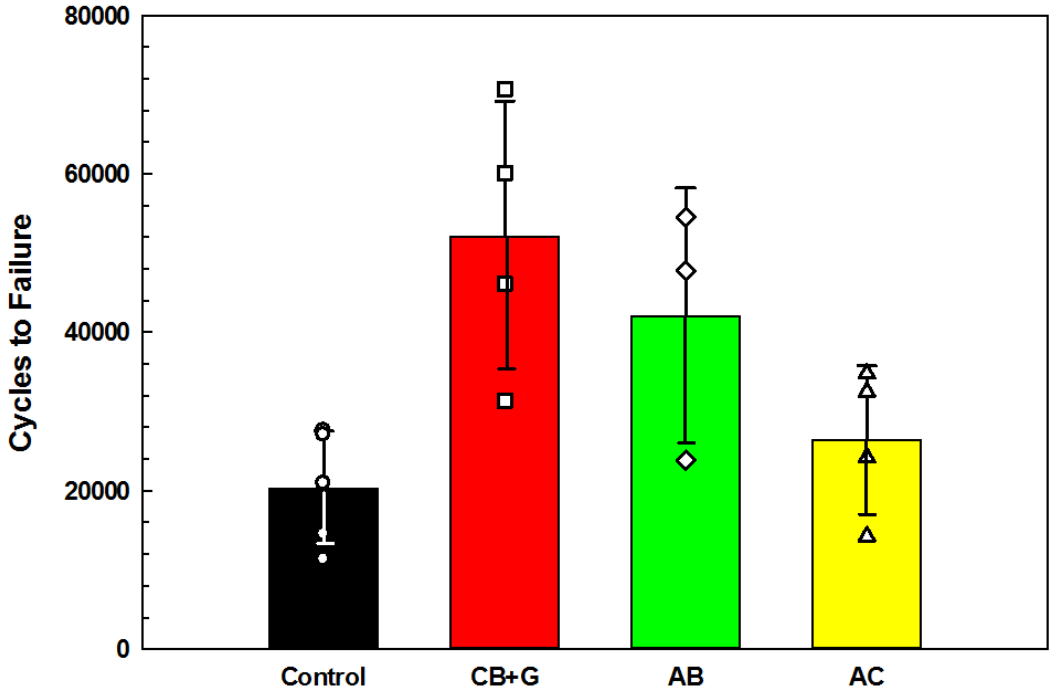

Figure 26: Cycle life for control, carbon black+graphite, acetylene black, and activated carbon containing cells. The solid bars indicate the average cycle life and the error bars one standard deviation. Also shown are the individual data points for each battery type.

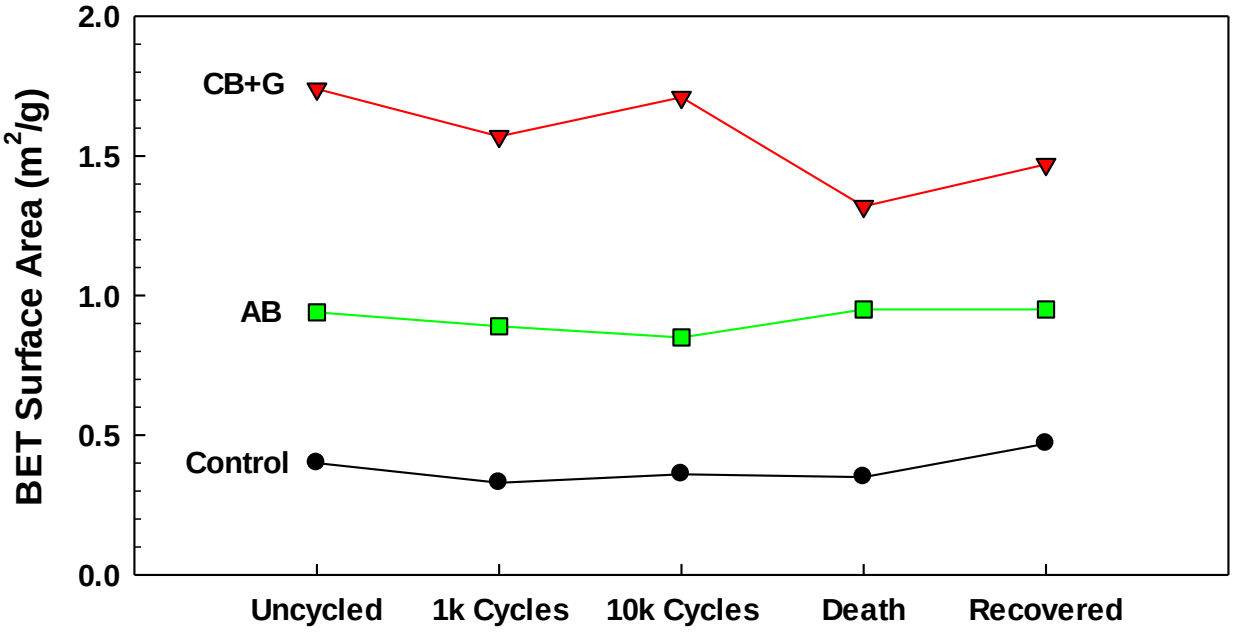

Figure 27: BET surface area for control cells, activated carbon containing cells, and acetylene black containing cells. BET surface area remained constant from activation of until death of the cells, including cells where the cycle life was extended through recovery charges.

Table 9: BET Porosity for Batteries Cycled to Failure With and Without Recovery Charges

	% Porosity	
	At Failure	With Recovery
Control	43.6	45.7
Activated Carbon	27.7	
Acetylene Black	49.0	53.9
Carbon Black + graphite	38.7	47.3

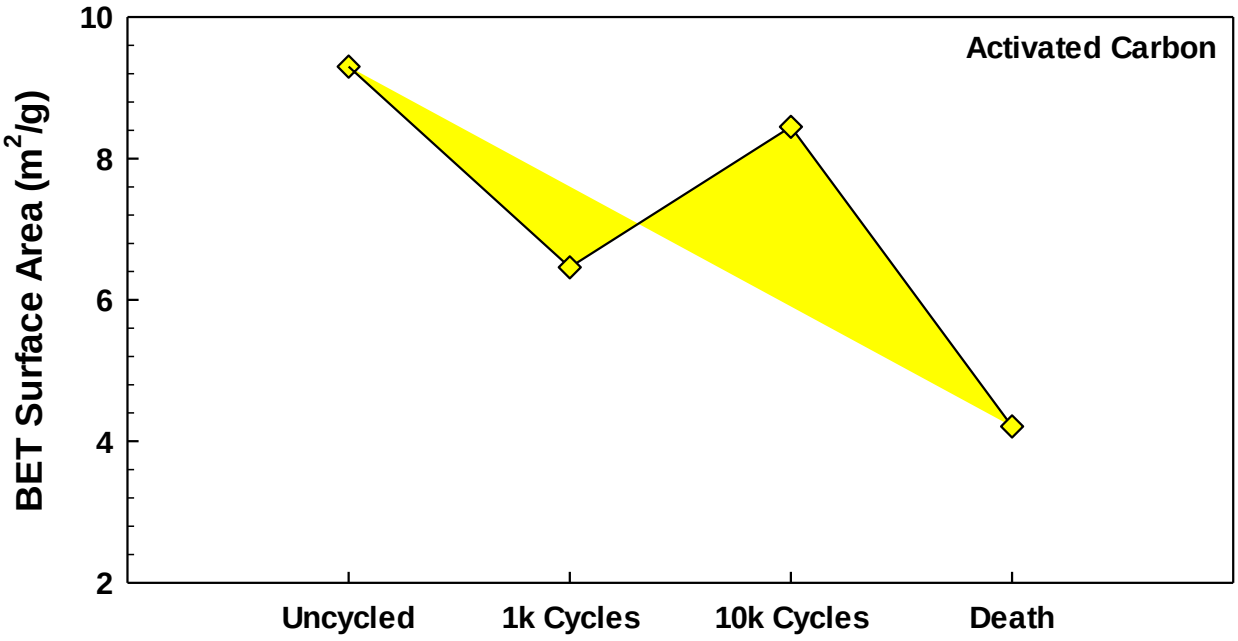

Figure 28: BET surface area for activated carbon containing cells as a function of cycle life. Unlike the other cells, the surface area decreased as the cells were cycled to death.

The addition of periodic recovery charges whenever the battery capacity had fallen below 80% of its initial capacity resulted in a substantial increase in cycle life, as discussed above. Evaluation of the plates from samples which failed after repeated recovery charges via mercury porosimetry revealed a substantial difference from samples which were not subjected to a recovery charge. As illustrated in Figure 30, the control, acetylene black, and carbon black + graphite cells had a very similar pore structure. As with the unrecovered cells, the pore size distribution peaked at approximately 1 micron. In addition, consistent with cross sectional analyses of the plates, a more significant distribution of very large pores (greater than 100 microns in diameter) was present for all of the cells, whereas for the unrecovered batteries this was observed primarily in the acetylene black containing cells.

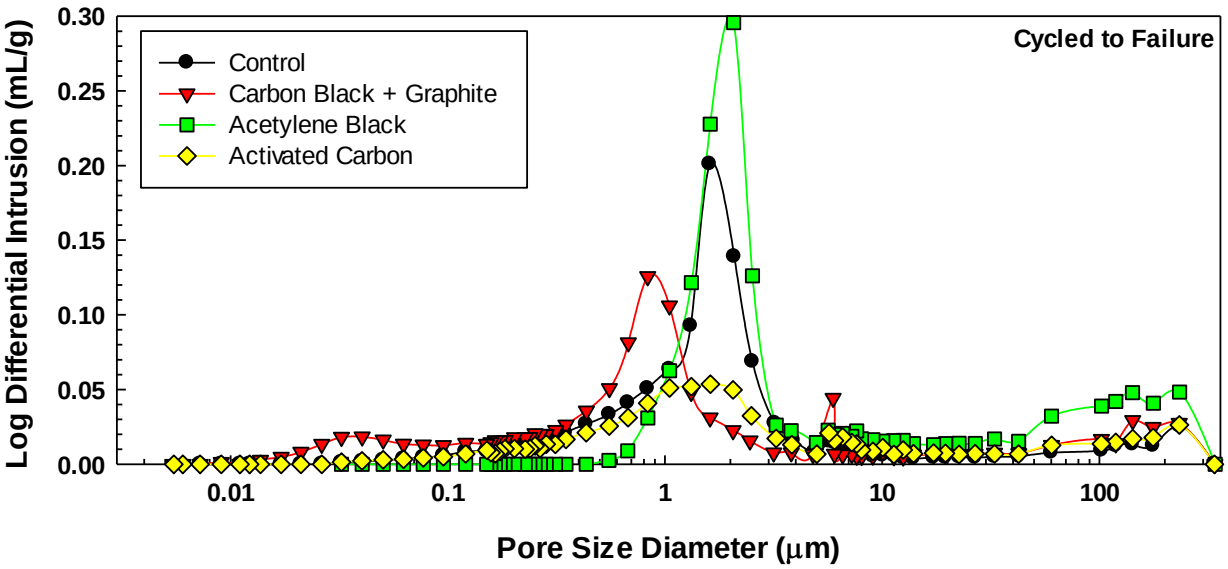

Figure 29: Intrusion rate as a function of pore size diameter, illustrating the distribution of pores found in each formulation after being cycled to failure.

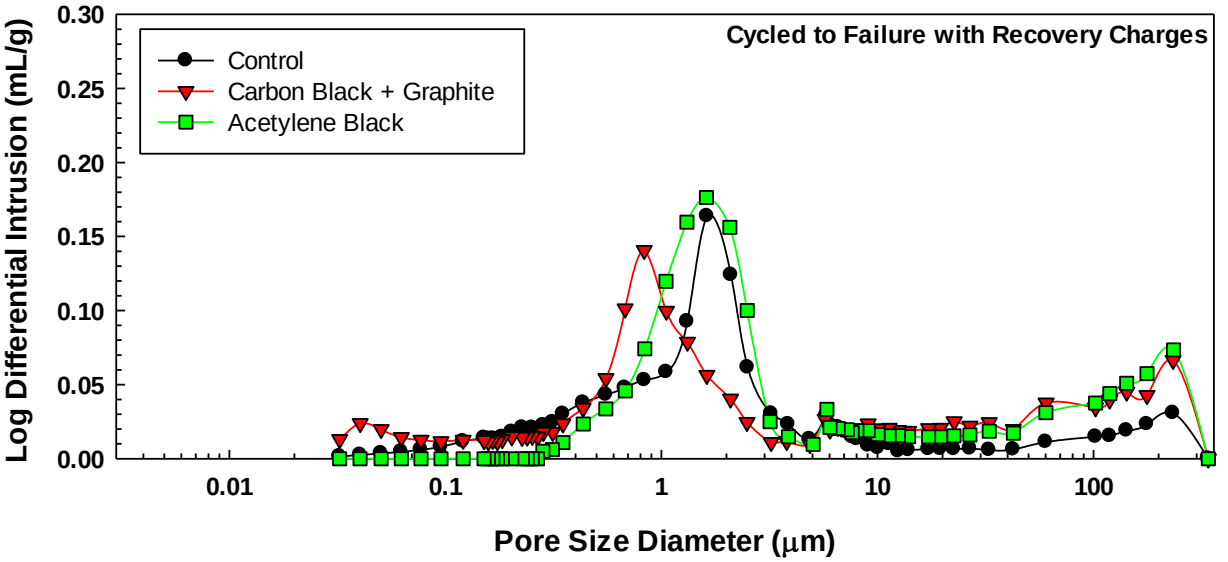

Figure 30: Intrusion rate as a function of pore size diameter, illustrating the distribution of pores found in each formulation after being cycled to failure with the incorporation of a recovery charge each time the capacity fell below 80% of the initial capacity.

In the next four figures, a comparison of the pore structure as a function of cycle life for each of the battery compositions is presented. Looking first at the control cells (Figure 31), the pore structure is seen to evolve as the battery is cycled. Initially, the majority of the pores are approximately 10 microns in diameter. As the batteries were cycled, the pore structure appeared to remain relatively constant, with a large distribution of pores remaining at approximately 10 microns. At failure, a marked reduction in the pore size was observed, with the distribution centered at a diameter nearly an order of magnitude lower.

The pore structure as a function of cycle life for activated carbon containing cells is illustrated in Figure 32. Throughout the cycle life of these cells a bimodal distribution of pores was present, with one

population similar to that of the control cells at approximately 10 microns, and a second closer to 3 microns. As the battery was cycled, the distribution shifted towards the smaller pores, with the majority being at the smaller size. At failure, the distribution was nominally identical to that of the control cell, with a distribution centered around approximately 1 micron.

The carbon black containing cells exhibited a markedly different behavior than the control or activated carbon containing cells. In the acetylene black containing cells (Figure 33), while the as-formed (i.e., uncycled) plates had a sizeable fraction of pores with a diameter centered around 10 microns, this distribution went away upon cycling, with the entire distribution of pores being centered around 1 to 3 microns. This remained true from 1000 cycles all the way until failure of the cell, and coupled with the dramatically improved cycle life when compared to the control cells (Figure 26) illustrates that the typical pore size, in and of itself, does not dictate battery performance. Another differentiating characteristic between the acetylene black containing cells and the control or activated carbon containing cells is the development of a volume fraction of large pores (100 microns and larger) as the cells approached end of life. This observation is consistent with cross sectional analyses that also illustrated the presence of these larger voids in the active material.

The behavior of the carbon black plus graphite cells is illustrated in Figure 34. Unlike the acetylene black containing cells, even in the as-formed condition, the pore structure was centered around 1 micron, with no distinct distribution at larger sizes. As the cells were cycled, the distribution remained centered around approximately 1 micron. A small distribution of very large pores (100 microns and larger) was present in these cells; however, the quantity did not appear to change markedly over the cycle life of the battery.

The observations from these cells, coupled with those of the acetylene black containing cells, suggest that the carbon black acts to stabilize the pore structure of the batteries, resisting substantial structural evolution. Furthermore, the lack of any distinct change in the negative plates for the carbon containing cells, either structurally (in terms of the nature of the pores in the active material) or chemically (in terms of substantial formation of $PbSO_4$ within or on the surfaces of the negative plates) suggests that the positive plates may be what is limiting the capacity of the cells as they approach failure. To explore this, a positive plate in the as-formed condition as well as after 10,000 cycles and 50,000 cycles (failure for this particular battery) were cross sectioned. The two cycled plates were taken from carbon black plus graphite containing cells.

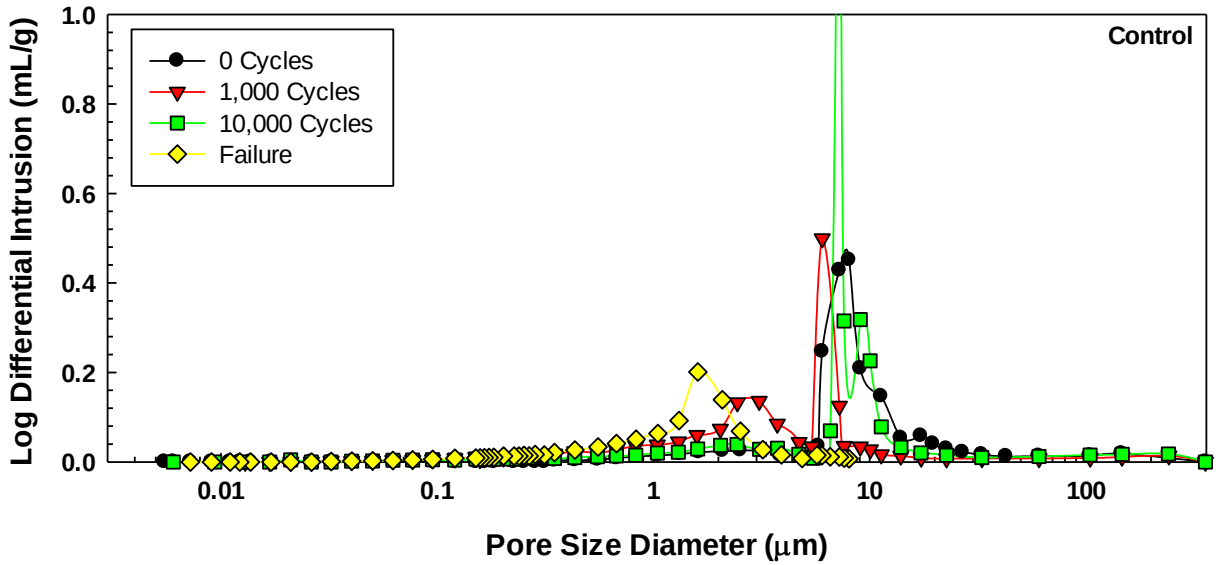

Figure 31: Intrusion rate as a function of pore size diameter, illustrating the distribution of pores found

in control cells from activation (0 cycles) through failure.

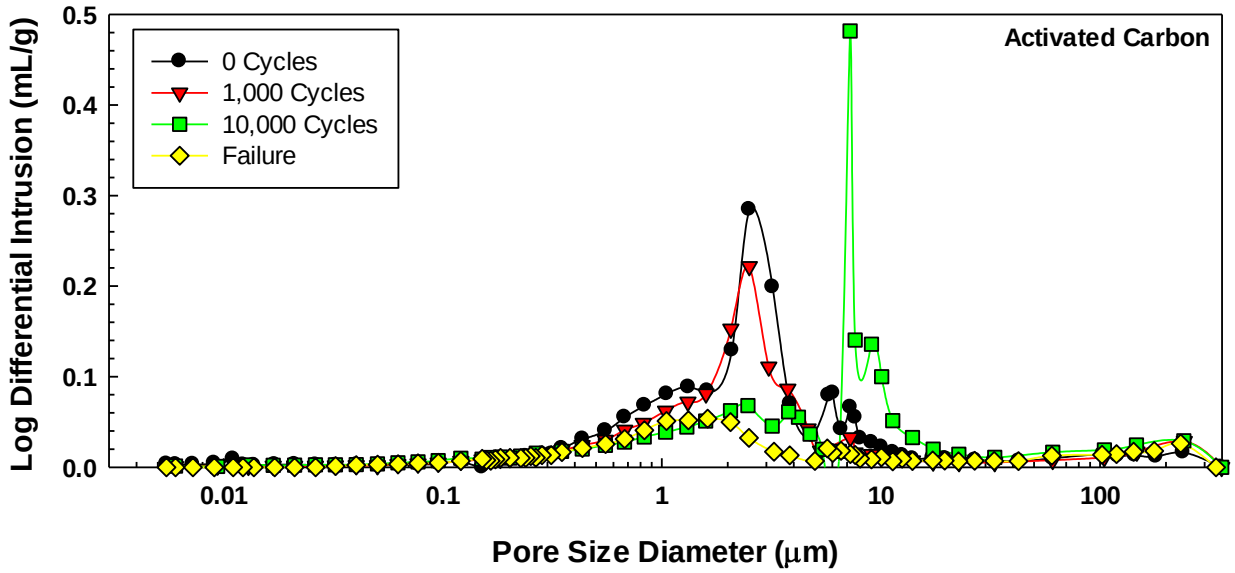

Figure 32: Intrusion rate as a function of pore size diameter, illustrating the distribution of pores found in activated carbon containing cells from activation (0 cycles) through failure.

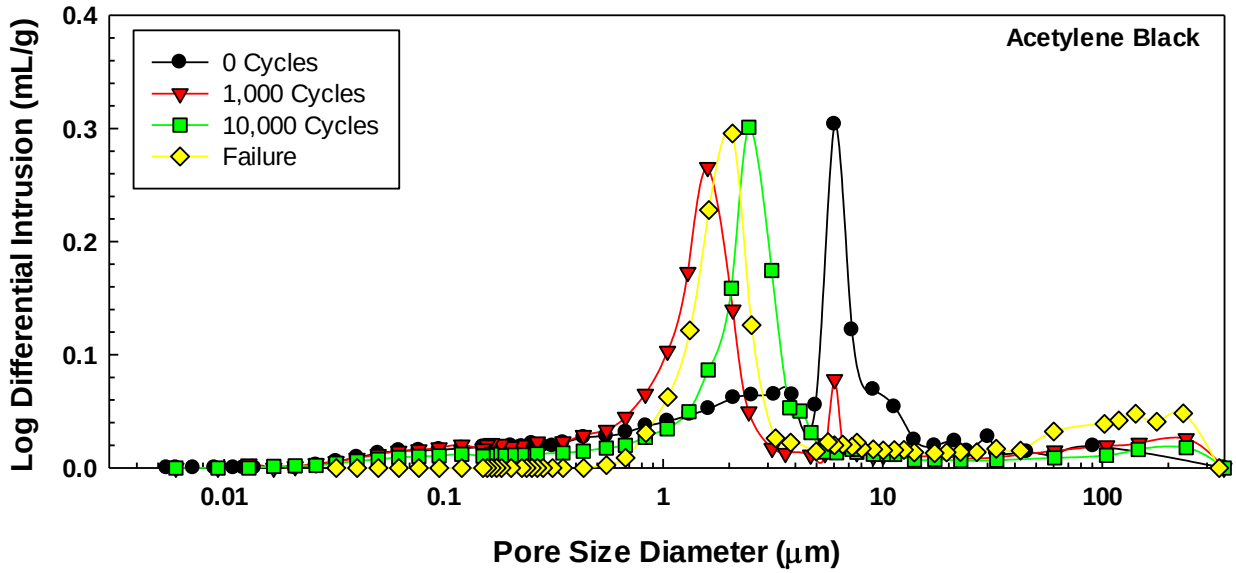

Figure 33: Intrusion rate as a function of pore size diameter, illustrating the distribution of pores found in acetylene black containing cells from activation (0 cycles) through failure.

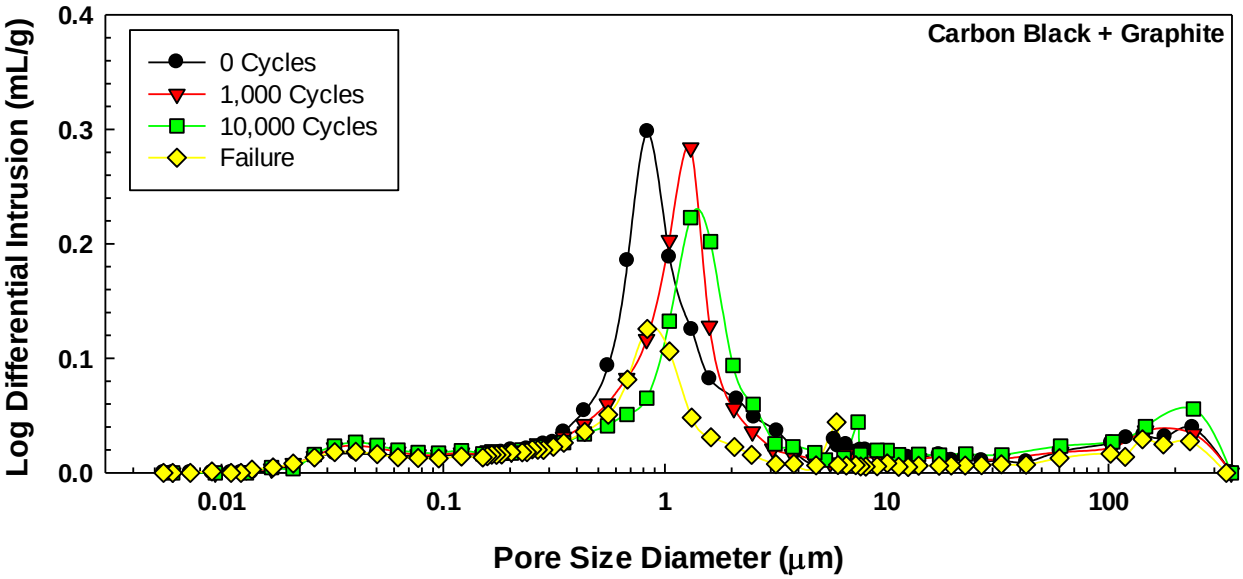

Figure 34: Intrusion rate as a function of pore size diameter, illustrating the distribution of pores found in carbon black + graphite containing cells from activation (0 cycles) through failure.

In Figure 35, a cross sectional view of an as-formed (i.e., uncycled) positive plate is presented. As can be seen, the structure differs from that of the negative plates in that it appears to be less porous, and the metallic lead more continuous in nature. Cathodoluminescence did not reveal the presence of any $PbSO_4$ deposits within the plate at any of the positions evaluated. In Figure 36, a series of cross sectional views of a cycled positive plate early in its functional life, in this case taken from a carbon black plus graphite cell after a total of 10,000 cycles, is shown. Several structural changes are immediately apparent when compared to the uncycled plate. First, the structure of the metallic lead is becoming finer, and more globular in nature. In addition, occasional large $PbSO_4$ particles are apparent throughout the plate (Figure 36B) as well as a distribution of smaller particles (Figure 36D and F). However, it does not appear that the structure is being blocked or otherwise altered such that mass transport into the plate would be significantly hindered.

In Figure 37, a cross sectional view of a positive plate from a battery which had failed is presented. As with the previous example, this plate was taken from a carbon black plus graphite containing cell. In this case, the cell had been subjected to 50k cycles and had failed (i.e., capacity was less than 80% of the initial capacity). Structurally, the plate is very similar to the one observed at 10k cycles. The structure has continued to become finer, and more globular in nature. In addition, large $PbSO_4$ particles are clearly visible within the plate (Figure 37A); however, the volume fraction appears to be small based upon the cross sections evaluated for this study. Finally, looking at the overall structure, while there are regions where a distribution of $PbSO_4$ particles is visible, in much of the plate, not $PbSO_4$ was visible via cathodoluminscence. Based upon these observations, it does not appear that degradation of the positive plate is leading to failure of the cells.

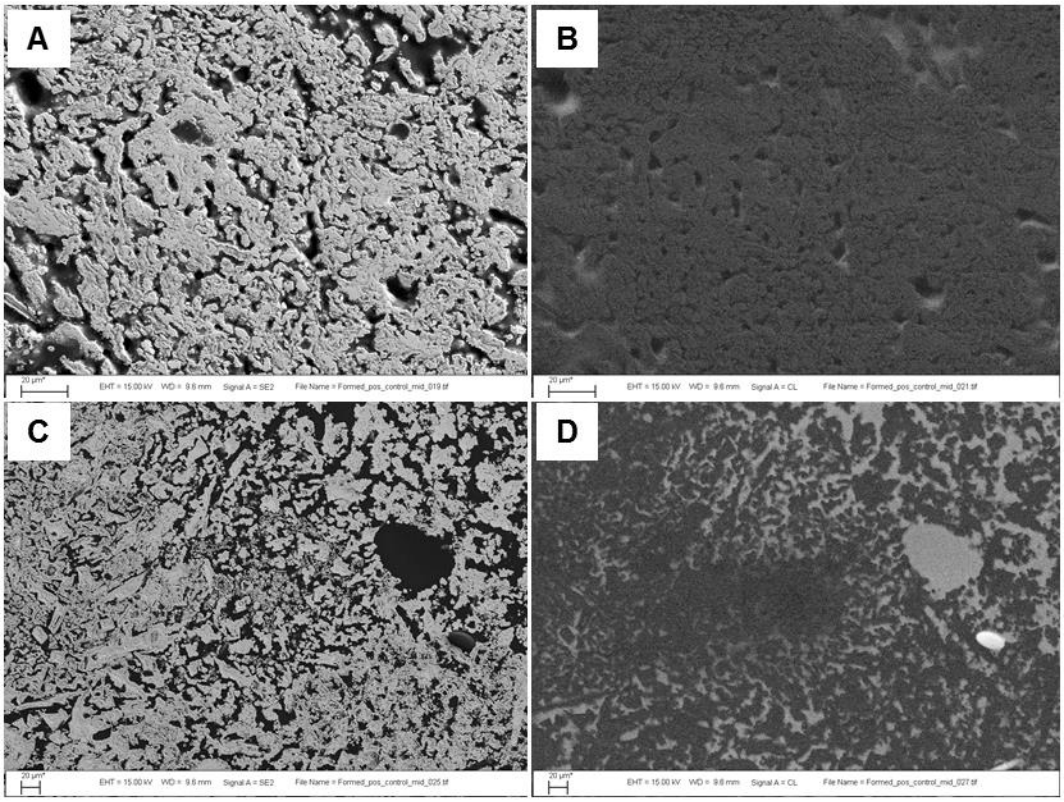

Figure 35: Cross sectional analysis of an as-formed (i.e., uncycled) positive plate. Two typical regions are shown, secondary electron images (A and C) and their corresponding cathodoluminescence images (B and D) illustrating the lack of significant lead sulfate formation.

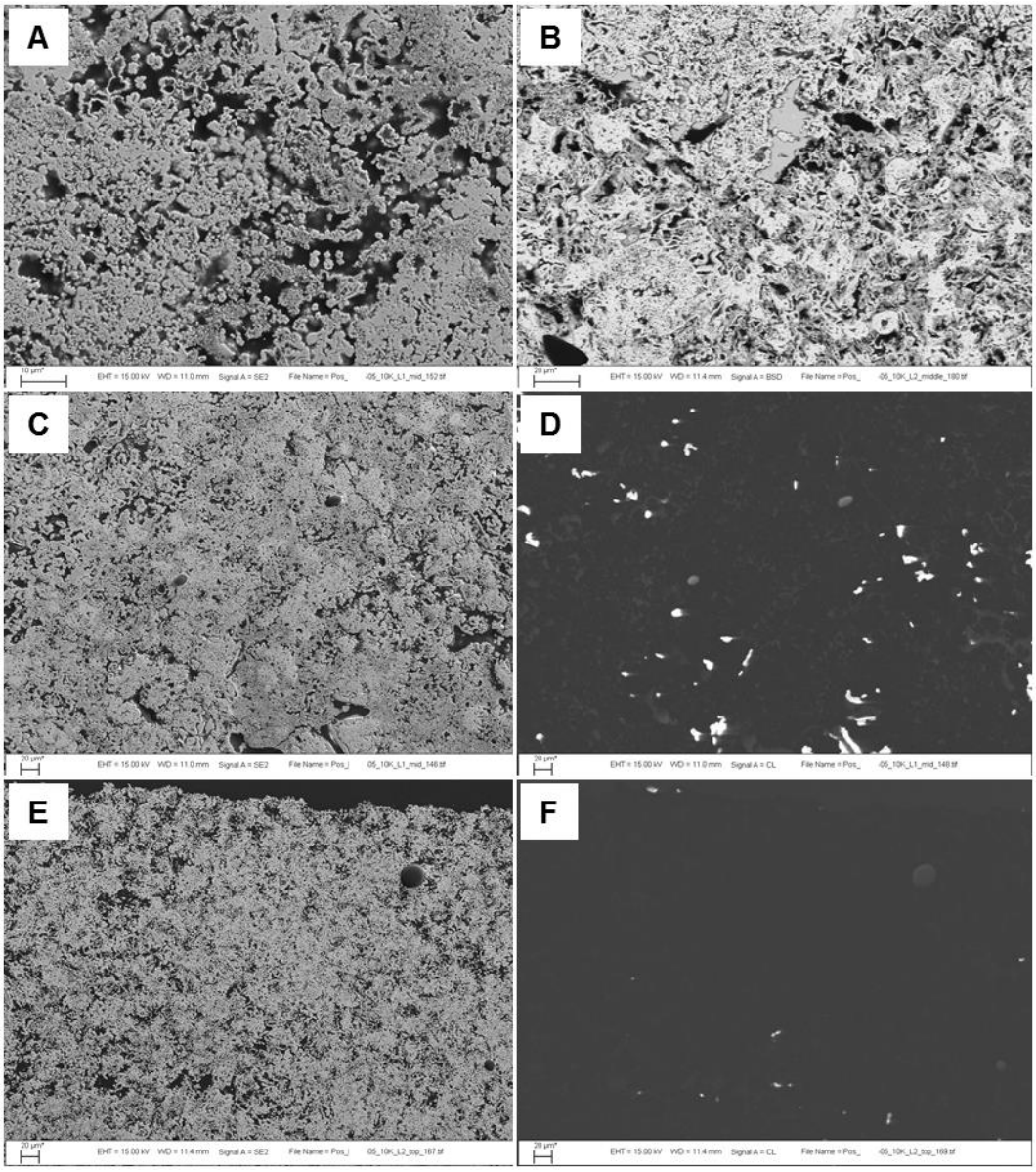

Figure 36: Cross sectional analysis of an cycled (10k cycles) positive plate taken from a carbon black + graphite cell. Two high magnification views are shown, illustrating the transition to an increasingly globular structure (A and B), along with two lower magnifcation views with secondary electron images (C and E) and their corresponding cathodoluminescence images (D and F) illustrating the formation of $PbSO_4$.

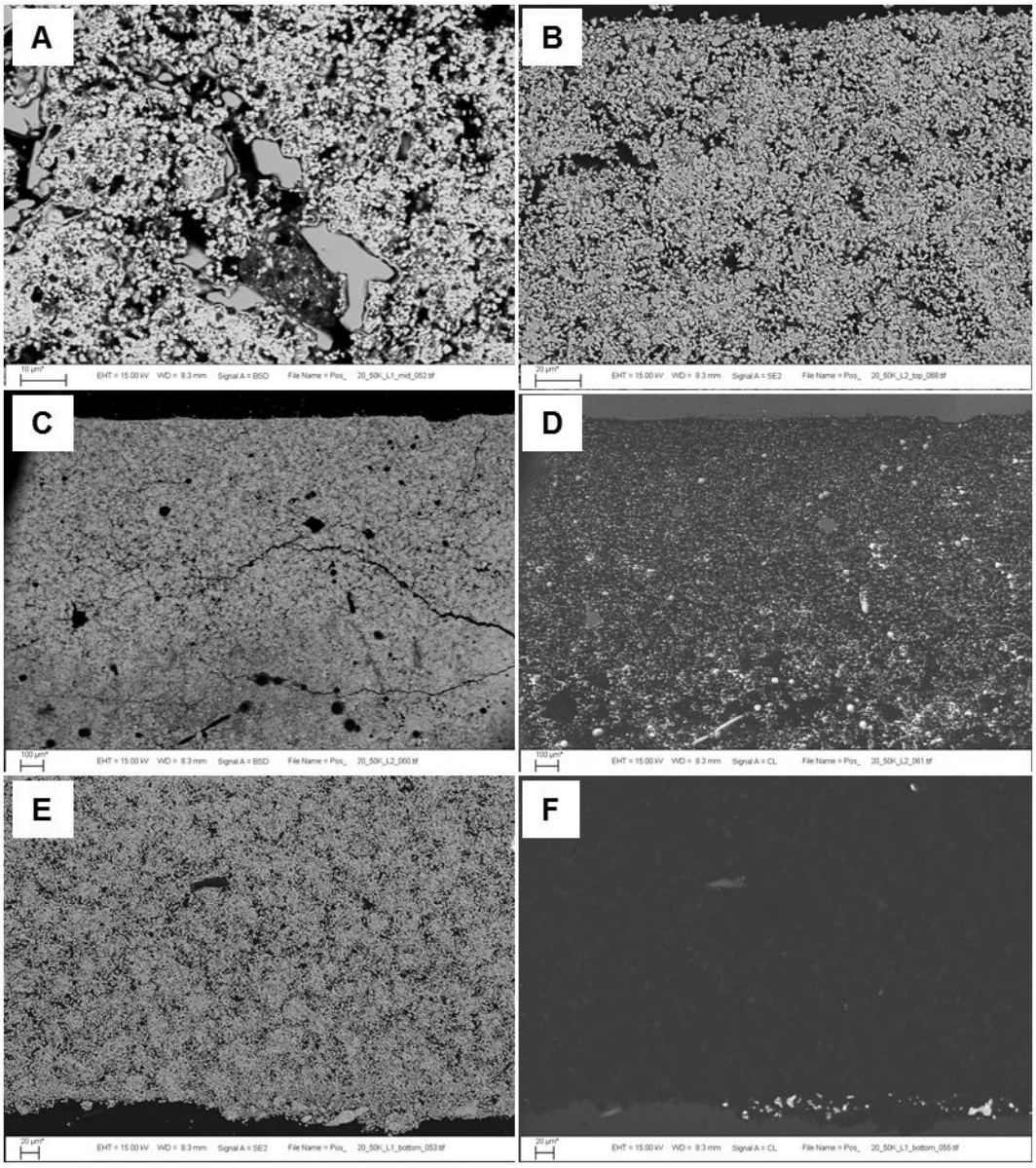

Figure 37: Cross sectional analysis of a cycled (50k cycles) positive plate taken from a carbon black + graphite cell. Two high magnification views are shown, illustrating the transition to an increasingly globular structure (A and B), along with two lower magnifcation views with secondary electron images (C and E) and their corresponding cathodoluminescence images (D and F) illustrating the formation of $PbSO_4$.

SUMMARY AND CONCLUSIONS

In this work, control cells along with three different carbon modified cells were evaluated under a range of conditions, from basic electrochemical performance through high rate, partial state of charge cycling. The physical and chemical changes taking place within the plates were monitored and an effort made to correlate performance to those changes. Batteries of all four chemistries were subjected to HRPSoC cycling and evaluated as a function of cycle life.

- The initial capacity of the carbon containing cells was slightly reduced relative to the control cell due to the lower active material content. In addition, the distribution of capacities was broader for the carbon containing cells, possibly due to the production process not being completely optimized.
- The float current for all of the carbon containing cells was greater than that of the control. This was likely due to the carbon, the surface area of which acted as a more effective cathode for water reduction than the metallic lead in the remainder of the negative active material.
- The level of self-discharge at 6 months was considerably larger for the carbon containing cells. This again was likely the result of the carbon serving as an effective cathode within the negative active mass, facilitating discharge
- Carbon additions universally improved the cycle life of the batteries under HRPSoC operation. The greatest improvement was observed for the carbon black plus graphite containing cells, followed by the acetylene black and then activated carbon containing cells.
- BET surface area was constant for the control, carbon black plus graphite, and acetylene black containing cells across their entire cycle life. The surface area decreased with cycles for the activated carbon containing cells, but was always much greater than the other battery chemistries.
- The pore structure for the control, acetylene black, and activated carbon containing cells all evolved over their cycle life, approaching a common distribution. The carbon black plus graphite containing cell remained relatively constant over its entire cycle life
- Analysis of positive plates from as received and cycled cells revealed that the positive plate was not leading to failure of the cells, and that the negative active material was likely dominating the behavior.

REFERENCES

Boden, D., Loosemore, D., Spence, M., & Wojcinski, T. (2010). Optimization Studies of Carbon Additives to Negative Active Materials for the Purpose of Extending the Life of VRLA Batteries in High-rate Partial-state-of-charge Operation. *Journal of Power Sources, 195*, 4470-4493.

Calábek, M., Micka, K., Křivák, P., Bača, P., Bilko, R., & Lábus, R. (2008). *Significance Of Carbon Additive In Negative lead-Acid Battery Electrodes.* ALABC.

Calebek, M., Micka, K., Krivak, P., & Baca, P. (2006). Significance of Carbon Additive in Negative Lead-acid Battery Electrodes. *Journal of Power Sources, 158*, 864-867.

DOE. (2003). *FreedomCAR Battery Test Manual for Power-Assist Hybrid Electric Vehicles.* DOE.

Fernandez, M., Valenciano, J., Trinidad, F., & Munoz, N. (2010). The Use of Activated Carbon and Graphite for the Development of Lead-acid Batteries for Hybrid Vehicle Applications. *Journal of Power Sources, 195*, 4458-4469.

Hund, T., Clark, N., & Baca, W. (2008). Ultrabattery Test Results for Utility Cycling Applications. *18th International Seminar on Double Layer Capacitors and Hybrid Energy Storage Devices.*

Kozawa, A., Oho, H., Sano, M., Brodd, D., & Brodd, R. (1999). Beneficial Effect of Carbon-PVA Colloid Additives for Lead-acid Batteries. *Journal of Power Sources, 80*, 12-16.

Lam, L., Louey, R., Haigh, N., Lim, O., Vella, D., Phyland, C., . . . Kano, T. (2007). *Production and test of hybrid VRLA Ultrabattery designed specifically for high-rate partial-state-of-charge operation.* Project DP 1.1, Final Report, ALABC.

Micka, K., Calábek, M., Bača, P., Křivák, P., Lábus, R., & Bilko, R. (2009). Studies of Doped Negative Valve-regulated Lead-acid Battery Electrodes. *Journal of Power Sources, 191*, 154-158.

Moseley, P. (2009). Consequences of Including Carbon in the Negative Plates of Valve-regulated Lead-acid Batteries Exposed to High-rate Partial-state-of-charge Operation. *Journal of Power Sources, 191*, 134-138.

Moseley, P., Nelson, R., & Hollenkamp, A. (2006). The Role of Carbon in Valve-regulated Lead-acid Battery Technology. *Journal of Power Sources, 157*, 3-10.

Ohmae, T., Hayashi, T., & Inoue, N. (2003). Development of 36-V Valve Regulated Lead-acid Battery. *Journal of Power Sources, 116*, 105-109.

Pavlov, D., Nikolov, P., & Rogachev, T. (2010). Influence of Expander Components on the Processes at the Negative Plates of Lead-acid Cells on High-rate Partial-state-of-charge Cycling. Part II. Effect of Carbon Additives on the Processes of Charge and Discharge of Negative Plates. *Journal of Power Sources, 195*, 4444-4457.

Pavlov, D., Rogachev, T., Nikolov, P., & Petkova, G. (2009). Mechanism of Action of Electrochemically Active Carbons on Processes that Take Place at The Negative Plates of Lead Acid Batteries. *Journal of Power Sources, 191*, 58-75.

Sawa, K., Funato, T., Watanabe, M., Wada, H., Nakamura, K., Shiomi, M., & Osumi, S. (2006). Development of Additives in Negative Active-material to Suppress Sulfation during High-rate, Partial-state-of-charge Operation of Lead-acid Batteries. *Journal of Power Sources, 158*, 1084-1090.

Shiomi, M., Funato, T., Nakamura, K., Takahash, K., & Tsubota, M. (1997). Effects of Carbon in Negative Plates on Cycle-life Performance of Calve-regulated Lead/Acid Batteries. *Journal of Power Sources, 64*, 147-152.

Spence, M. A., Boden, D. P., & Wojcinski, T. D. (2008). *Identification of the Optimum Specification for Carbon to be Included in the Negative Active Material of a Valve-Regulated Battery in Order to Avoid Accumulation of Lead Sulfate During High-Rate Partial-State-of-Charge Operation.* ALABC.

Spence, M. A., Boden, D. P., & Wojcinski, T. D. (2009). *Identification of the Optimum Specification for Carbon to be Included in the Negative Active Material of a Valve-Regulated Battery in Order to Avoid Accumulation of Lead Sulfate During High-Rate Partial-State-of-Charge Operation.* ALABC.

Valenciano, J., Sanchez, A., Trinidad, F., & Hollenkamp, A. (2006). Graphite and Fiberglass Additives for Improving High-rate Partial-state-of-charge Cycle Life of Valve-regulated Lead-acid Batteries. *Journal of Power Sources, 158*, 851-863.

Walmet, P. (2009). *Evaluation of Lead/Carbon Devices for Utility Applications.* Sandia National Laboratories.

DISTRIBUTION

Name	Org.	Mail Stop
Imre Gyuk	DOE Office of Electricity Energy Storage Systems Program Manager U.S. Department of Energy 1000 Independence Avenue, SW Washington, DC 20585	
Rod Shane	East Penn Manufacturing Deka Road Lyon Station, PA 19536	
David Enos	1818	0888
Summer Ferreira	2546	0614
Karen Waldrip	2546	0614
Tom Wunsch	2546	0614
Ross Guttromson	6113	1108
Technical Library	9536	0899
OFA/NFE Agreements	10012	0115


Sandia National Laboratories